Bioactive Materials 8 (2022) 478–493

Contents lists available at ScienceDirect

Bioactive Materials

journal homepage: www.sciencedirect.com/journal/bioactive-materials

Nano-hydroxyapatite accelerates vascular calcification via lysosome impairment and autophagy dysfunction in smooth muscle cells

Qi Liu [a,1], Yi Luo [a,1], Yun Zhao [b,a], Pingping Xiang [a], Jinyun Zhu [a], Wangwei Jing [a], Wenjing Jin [c], Mingyao Chen [a], Ruikang Tang [c,**], Hong Yu [a,*]

[a] Department of Cardiology, Cardiovascular Key Laboratory of Zhejiang Province, The Second Affiliated Hospital, Zhejiang University School of Medicine, Hangzhou, Zhejiang Province, 310009, China
[b] The Affiliated Cardiovascular Hospital of Qingdao University, Qingdao, Shandong Province, 266071, China
[c] Department of Chemistry, Zhejiang University, Hangzhou, Zhejiang Province, 310027, China

ARTICLE INFO

Keywords:
Nano-hydroxyapatite
Vascular calcification
Autophagy
Lysosome
Exosome

ABSTRACT

Vascular calcification (VC) is a common characteristic of aging, diabetes, chronic renal failure, and atherosclerosis. The basic component of VC is hydroxyapatite (HAp). Nano-sized HAp (nHAp) has been identified to play an essential role in the development of pathological calcification of vasculature. However, whether nHAp can induce calcification in vivo and the mechanism of nHAp in the progression of VC remains unclear. We discovered that nHAp existed both in vascular smooth muscle cells (VSMCs) and their extracellular matrix (ECM) in the calcified arteries from patients. Synthetic nHAp had similar morphological and chemical properties as natural nHAp recovered from calcified artery. nHAp stimulated osteogenic differentiation and accelerated mineralization of VSMCs in vitro. Synthetic nHAp could also directly induce VC in vivo. Mechanistically, nHAp was internalized into lysosome, which impaired lysosome vacuolar H^+-ATPase for its acidification, therefore blocked autophagic flux in VSMCs. Lysosomal re-acidification by cyclic-3′,5′-adenosine monophosphate (cAMP) significantly enhanced autophagic degradation and attenuated nHAp-induced calcification. The accumulated autophagosomes and autolysosomes were converted into calcium-containing exosomes which were secreted into ECM and accelerated vascular calcium deposit. Inhibition of exosome release in VSMCs decreased calcium deposition. Altogether, our results demonstrated a repressive effect of nHAp on lysosomal acidification, which inhibited autophagic degradation and promoted a conversion of the accumulated autophagic vacuoles into exosomes that were loaded with undissolved nHAp, Ca^{2+}, Pi and ALP. These exosomes bud off the plasma membrane, deposit within ECM, and form calcium nodules. Vascular calcification was thus accelerated by nHAP through blockage of autophagic flux in VSMCs.

1. Introduction

Vascular calcification (VC) is a detrimental pathology highly prevalent in aging, diabetes mellitus, atherosclerosis, and chronic renal failure. Development of VC involves aberrant calcium deposition in the vessel wall, apoptosis of vascular smooth muscle cells (VSMCs) and the phenotypic transformation of VSMCs into osteoblast-like cells [1,2]. During calcification, cytoplasmic Ca^{2+} and phosphate (Pi) incorporate with alkaline phosphatase (ALP) into exosomes that bud off the plasma membrane and associate with extracellular proteins, such as collagen. Crystals in the exosomes finally grow into nano-sized hydroxyapatite (nano-HAp or nHAp) [$Ca_{10}(OH)_2(PO_4)_6$] [3]. Studies have shown that nHAp stimulated osteogenic transdifferentiation of SMCs in vitro and induced calcification on extracellular matrix (ECM) [4–6], but there was no experimental result in vivo. The previous studies suggested that nHAp may lead to a pathological feedback loop causing more inflammation, cell death, phenotypic change, matrix degradation, and calcification. This may explain why calcification progresses rapidly once

Peer review under responsibility of KeAi Communications Co., Ltd.
* Corresponding author. Department of Cardiology, Second Affiliated Hospital, Zhejiang University School of Medicine, 88 JieFang Rd, Hangzhou, 310009, China.
** Corresponding author. Department of Chemistry, Zhejiang University, Hangzhou, 310027, China, ZheDa Road, NO.38.
E-mail addresses: rtang@zju.edu.cn (R. Tang), yuvascular@zju.edu.cn (H. Yu).
[1] These authors contributed equally to the manuscript.

https://doi.org/10.1016/j.bioactmat.2021.06.004
Received 26 January 2021; Received in revised form 20 May 2021; Accepted 2 June 2021
Available online 14 June 2021

microcalcification exists. Whether nHAp can induce calcification in vivo and the underlying mechanism by which nHAp affects the VSMCs remain unclear.

Autophagy is a "housekeeping" subcellular process for lysosome-mediated turnover of damaged cytosolic materials that are engulfed by a double membraned phagophore to form an autophagosome. The autophagosomes fuse with single membraned acidic lysosomes to form autolysosomes, where the engulfed content is degraded and recycled [7]. Autophagy has been shown to regulate Ca^{2+} homeostasis in VSMCs. Studies proved that autophagy dysfunction contributes to VC [8,9]. These studies demonstrated a protective role of autophagy in vascular disorders. Mice with VC had increased expression of the autophagy markers microtubule-associated light chain 3 II (LC3-II) and sequestosome 1 (SQSTM1/p62), etc. in aortic VSMCs as compared to that in normal mice [10]. Evidence also demonstrated that increased cytosolic concentrations of Ca^{2+} induced autophagosome accumulation, which was caused by a decline in autophagic clearance via lysosomes [11,12]. These studies indicated that impaired autophagy may contribute to VC, and lysosomal function may involve in VC. These data suggest that autophagy-lysosomal function plays an important regulatory role in vascular calcification.

Lysosomes are single membrane-enclosed organelles present in all eukaryotic cells that contain large numbers of hydrolytic enzymes. Lysosomes exhibit their maximal enzymatic activity at a low pH ($pH \leq 5$) and digest extracellular material from the endocytic pathway and intracellular material from the autophagic pathway. Disorders of lysosome acidification disrupt the clearance of autophagy [13]. Nanoparticles could lead to impairment of both autophagy and lysosome [14]. However, whether and how nHAp affects autophagy and lysosome in VSMCs remain to be elucidated.

Recently, secretary autophagy as a new concept was presented in addition to the traditional degradative autophagy [15]. Autophagic proteins were found on matrix vesicles (MVs) that were secreted out of cells [15]. MV membranes are enriched in phosphatidylethanolamine [16,17] which is also a main constituent of the mature autophagosome membrane [18]. These data suggest that autophagic vesicles can form MVs to be released into matrix outside of cells. In addition, one study proved that the calcium-containing MVs in osteoblasts were transported via lysosome and secreted by exocytosis, indicating that lysosome plays a central role in mineralization [19]. Studies have shown that MVs are enriched with a concoction of calcifying enzymes and crystals of calcium phosphate HAp mineral [16,20]. Such MVs are released from osteogenic cells and facilitate HAp formation in ECM [21]. In context of atherosclerosis, VSMCs and macrophages are the primary source of these calcified MVs which are released into the collagen rich matrix in the intima to promote atherosclerotic calcification, directly leading to the formation of calcified plaques [22]. It is reasonable to speculate that MVs may be entwined with the network of autophagic vesicles either at the stage of their formation or release during the process of vascular calcification. Accumulating evidence indicates that matrix vesicles are secreted from multivesicular bodies and are enriched with the exosome markers CD63, CD9, CD81, and MHC I. Secretion of these exosome-like structures is regulated by sphingomyelin phosphodiesterase 3, and inhibition of this enzyme prevents vascular calcification [23]. Comparative proteomics showed that VSMC derived exosomes were compositionally similar to exosomes from other cell sources but also shared components with osteoblast-derived MVs including calcium-binding and extracellular matrix proteins [24]. Despite the clinical importance of exosomes in triggering vascular calcification, little is known of the link between exosomes biogenesis and VC induced by nHAp.

In this study, we demonstrated that nHAp accelerated VC through lysosomal impairment and blockage of autophagy flux in VSMCs and enhanced the release of calcifying-exosomes. We for the first time illustrated the effect of autophagy-lysosome impairment on VC, and highlighted the link between nHAp-induced deficiencies of lysosome activity and calcium deposition of VSMCs.

2. Methods and materials

2.1. Characterization of nanoparticles

Synthetic nHAp (purity 97%; particle size less than 100 nm) was obtained from Aladdin Biochemical Technology (Shanghai, China). Human-derived HAp crystals were prepared from samples of human carotid arteries removed by endarterectomy. The HAp crystals were dissected as described previously [25]. The hardened, obviously calcified regions were dissected from the atherosclerotic vessels and digested with collagenase (3 mg/mL) and elastase (1 mg/mL) overnight at 37 °C. After digestion, the crystals were washed 3 times in Hanks' Balanced Salt Solution. Samples were then placed on a 70-μm sieve (Gibco) and washed further. The remaining crystals (>70 μm) were crushed using a pestle and mortar into Hanks' Balanced Salt Solution. Washing of the crystals at this stage was achieved using ultracentrifugation at 100000 g to capture very small particles. The morphology and size of the crystals were characterized by scanning electron microscope (SU8010, HITACHI, Japan). The phase composition of the prepared nano-sized crystals was confirmed by X-ray diffraction (XRD, PANALYTICAL, The Netherlands) with Cu-Kα radiation and Fourier transform infrared (FT-IR) spectroscopy (FITR-8400S, SHIMADZU, Japan).

2.2. Cell culture

Vascular SMCs were isolated from aortas of 8-week-old wild-type C57BL/6 mice (Slac Laboratory Animal). Briefly, the adventitia and endothelium were removed and the median layers were digested with 1 mg/mL collagenase type I (Worthington) and 0.714 U/mL elastase (Worthington) for about 1.5 h at 37 °C. Cells were maintained in Dulbecco's modified Eagle's medium (Hyclone) containing 20% fetal bovine serum (Hyclone) and 100 U/mL penicillin, 100 mg/mL streptomycin at 37 °C in a humidified atmosphere with 5% CO_2. Cells were used between passage 3–5 in the experiments. To determine the effect of nHAp on VSMCs in vitro, 1 mg/mL nHAp cyrstals in DMEM were dispersed with an ultrasonic vibrator. 100uL nHAp (1 mg/mL) suspension was added to 900uL DMEM, beaten and diluted to a final concentration of 100ug/mL. Then they were added to culture plate with cells. To compare the effects of osteogenic medium (OM) and nHAp on VSMCs, VSMCs were treated with OM containing 10 nmol/L dexamethasone (Sigma-Aldrich), 0.25 mmol/L L-ascobic acid (Sigma-Aldrich), 10 mmol/L β-glycerophosphate (Sigma-Aldrich), or/and 100 μg/mL nHAp for 24 h, then washed with phosphate-buffered saline (PBS) to remove nHAp, then continue to be cultured in OM or DMEM for 2 weeks.

2.3. Measurements of activity of alkaline phosphatase (ALP)

The ALP activity of VSMCs was determined by using a luminescence ALP detection kit in accordance with the manufacturer's instructions (Beyotime Biotechnology, Shanghai, China). After SMCs were cultured with 100 μg/mL HAp for 7 days, SMCs were washed with cold PBS, scraped into 100 μL of lysis buffer (0.2% NP-40 with l mM $MgCl_2$) and incubated for 30 min on ice. Then the lysis was centrifugated at 5000 rpm for 5 min and the supernatant was collected. All samples were stored under −80 °C until use for ALP assay which was performed following the manufacturer's instructions (Beyotime Biotechnology, Shanghai, China). By catalyzing p-nitrophenylphosphate (pNPP) to pNP, ALP activity is referred as the change of absorbance at 405 nm, and then normalized to the protein level. Unit Definition: One ALP DEA unit equals hydrolyzation of 1 mol of p-nitrophenyl phosphate per minute at pH 9.8 at 37 °C.

2.4. Alizarin Red staining

After cultured at specified conditions for 14 days, VSMCs on dishes were fixed with 10% formalin for 30 min, then washed with double distilled water (ddH_2O) twice and incubated with Alizarin Red (Solarbio Life Sciences, China) for 5 min and washed with ddH_2O twice to remove the excessive dye. After examination and photography under a microscopy, the dye on the cells was extracted with 100ul Hexadecyl Pyridinium chloride (Sigma-Aldrich) and the optical density (OD) at 560 nm was measured using a microplate reader (Spectra MAX 190, Molecular Devices, USA).

2.5. von kossa staining

A segment of the abdominal aorta was excised and fixed in 10% formalin for 24 h, then dehydrated, embedded in paraffin, and cut into 5-μm -thick sections. The slides were deparaffinized, dehydrated and washed in distilled water (ddH_2O),the samples were incubated with reagent A of von Kossa staining Kit (Solarbio Life Sciences, China) and placed under ultraviolet light for 10 min,and then placed into reagent B for 2 min followed by staining with hematoxylin for the demonstration of cell nucleus.

2.6. Acridine orange (AO) staining

VSMCs were exposed to 100 μg/mL nHAp for 24 h. The cells were then stained with 5 μg/mL acridine orange (Aladdin, China) for 20 min at 37 °C and 5% CO_2. Then the cells were washed with PBS, followed by the addition of DMEM without serum to the cells. The fluorescence images of the cells were immediately acquired on a fluorescence microscope (Leica).

2.7. Analysis of EGFR degradation

After treated with100 μg/mL nHAp for 24 h, VSMCs were incubated with serum-free DMEM containing 50 ng/mL of EGF for 0, 1, 2 and 3 h at 37 °C, and then the cells were either lysed and analyzed by western blot, or were fixed in 4% formaldehyde, stained with anti-EGFR antibody and imaged by fluorescence microscopy (Leica).

2.8. Lysosomal reacidification

To reacidify lysosome, a cAMP cocktail was used. It consisted of 500 μM 8-CPT-cAMP, 100 μM IBMX, and 10 μM forskolin.

2.9. Calcium quantification

To determine the calcium deposition in cells or exosomes, PBS-washed VSMCs on a dish or purified exosomes were dissolved in 100 μL 0.6 N HCl for 48 h. Calcium content was measured by Calcium Assay Kit (Cayman Chemical, USA). The amount of calcium was normalized to the total amount of protein or the number of cells.

2.10. Exosome isolation

Exosomes were harvested by following a modified Exosome isolation protocol [26]. Confluent VSMCs were washed twice with PBS and cultured with DMEM medium with S-HAp (100 μg/mL) for 3 days, and then the medium was collected and centrifuged at 10,000×*g* for 1 h to remove cells and apoptotic bodies. Exosomes were then harvested from the supernatant by centrifugation at 110,000×*g* for 70 min twice at 4 °C in an Ultracentrifuge (Optima L-90K; Beckman Coulter, USA). Exosomes were resuspended with PBS or 0.6 N HCl for protein or calcium content measurement, respectively. Exos were observed by TEM (Tecnai G2 spirit, Thermo FEI, USA) which demonstrated typical cup shapes with diameters around 100 nm (Fig S14A). Dynamic light scattering analysis further confirmed that the average diameter of Exos was approximately 133 nm (Fig S14B). Western blot confirmed the expression of the Exos' marker proteins Alix, TSG101 and CD9 in Exos, but no GAPDH expression. While the VSMCs have no expression of CD9. And the above markers all don't exist in the supernatants after ultracentrifugation (Fig S14C).

2.11. mRFP-GFP-LC3 adenovirus puncta assay

For the analysis of autophagic flux, VSMCs were transfected with stubRFP-sensGFP-LC3 Adenovirus (JIKAI, China) following the manufacturer's instructions. After 36 h, the transfected cells were starved or treated with 100 μg/mL S-HAp for 24 h. Then the cells were fixed with 4% paraformaldehyde in PBS and then stained with DAPI, and imaged using a fluorescence microscope (Leica, Germany).

2.12. Murine models of calcification

Two different murine models of calcification were created for this study. One is ectopic calcification on soft tissue inducing via injection of Matrigel mixed with GFP-labeled VSMCs and S-HAp. The other is by smearing HAp on the abdominal aorta. Mice (C57BL/6, 3-month old) were anesthetized with isoflurane. The mice were shaved and the skin was disinfected with 75% ethanol prior to operation. For the first one, three longitudinal skin incisions about 1 cm in length on the dorsal surface of each mouse were made, and subcutaneous pouches were created by blunt dissection. The implants were 400 μL in volume containing 5 mg S-HAp or 6×10^6 SMCs or both, which was thoroughly mixed in advance, and were placed into pouch as following: left pouch, 200 μL S-HAp + 200 μL Matrigel; right pouch, 100 μL S-HAp + 100 μL GFP-labeled SMCs+200 μL Matrigel; lower pouch, 200 μL GFP-labeled SMCs+200 μL Matrigel. The incisions were closed with surgical sewing. For the second model, a longitudinal skin incision about 2 cm in length on the abdominal surface of a mouse was made, and the abdominal aorta was isolated (between renal artery and the bifurcation of common iliac artery), the vascular adventitia was torn off. The artery was incubated with 0.9% NaCl, 0.5 M/L $CaCl_2$, or S-HAp (25 mg/mL 0.9% NaCl) for 15min with the aid of Stereo Microscope (SZ61, Olympus, Japan). The incisions were closed with surgical sewing. Calcification in vivo was evaluated using micro-CT (U-CT-OI, Milab, USA), belonging to Life Sciences Institute, Zhejiang University.

2.13. Statistical analysis

Data were expressed as means ± standard deviation (SD) and analyzed by Program Graph-Pad Prism version 6.0. Multiple comparisons were performed by one-way ANOVA followed by Bonferroni correction. A value of $p < 0.05$ was considered as statistically significant.

3. Results

3.1. Nano-sized hydroxyapatite exists in human calcified aorta

To study the relationship between nHAp and vascular calcification, human calcified aorta specimen was collected. Calcium deposition in both media and adventitia of the artery was detected (Fig. 1A). Nano-sized HAp was observed on the surface of the vascular cells by scanning electron microscope (SEM) (Fig. 1B). Energy dispersive spectrometer (EDS) of the dense structures under SEM revealed calcium and phosphorus, with small amounts of magnesium and carbon (Fig S2). The ratio of calcium to phosphorus was about 1.47. Interestingly, we found that nHAp was adhered to the VSMC surface and there was nHAp in the lysosome of the cell (Fig. 1C). In addition, abundant α-SMA positive cells expressing osteogenic marker Runx2 were observed on the calcified artery (Fig. 1D). These findings indicate that nHAp internalization

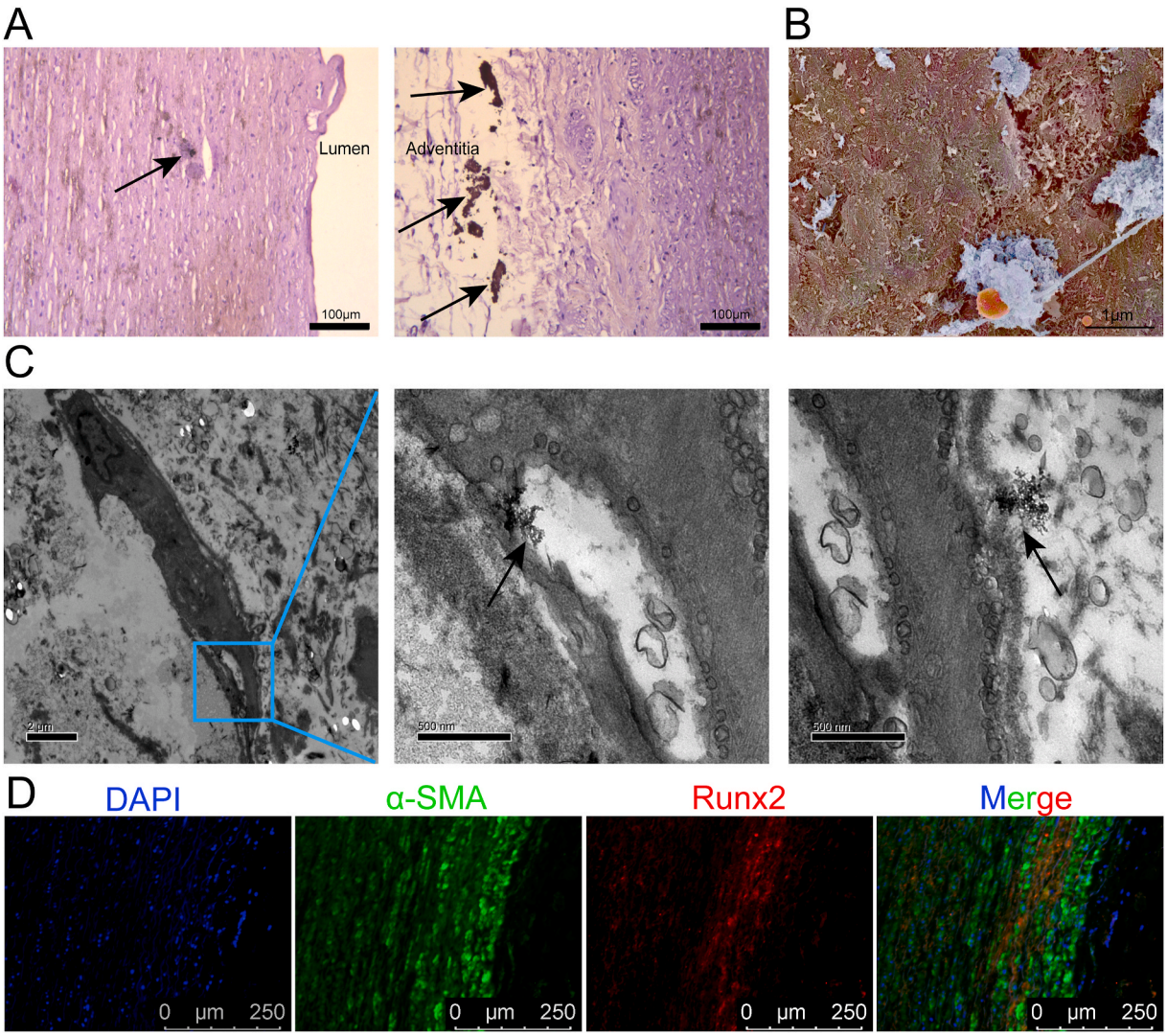

Fig. 1. Characterization of human calcified aorta. A) Representative images of the human aorta sections stained with von Kossa to detect calcium deposit (black arrows). Scale bar, 100 μm. B) Representative image of SEM showing HAp (Blue) on the surface of vascular cells (brown) in the calcified aorta. Scale bar, 1 μm. C) Representative images of TEM showing nano-sized HAp (black arrows) located intracellularly (middle) and extracellularly (right). Scale bar, 2 μm and 500 nm. D) Immunofluorescent staining of aorta sections shows expression of α-SMA and Runx2. Scale bar, 250 μm.

potentially contribute to the rapid progression of VC.

3.2. Characterization and cellular internalization of HAp crystals

To analyze the effect of HAp on calcification in VSMCs, we used synthetic nHAp (S-HAp) to mimic human naturally crystallized HAp (H-HAp) that was derived from atherosclerotic plaques of human aorta. The crystalline structures of synthetic and H-HAp crystals were similar in morphology under SEM (Fig. 2A), both were homogeneous and rod-like crystals. TEM analyses revealed that both the two kinds of crystals were near rod-like, and the size was about 100 nm (Fig. 2B). The X-ray diffraction (XRD) spectrum of synthetic and H-HAp crystals showed both had eight diffraction peaks of crystals (Fig. 2C), consistent with the standard HAp (JCPDS09-0432) [27]. The samples were further investigated by Fourier transform infrared spectrum (FT-IR) (Fig. 2D). Both crystals had the vibration peaks at 563, 603 and 1029 cm^{-1} which belonged to the asymmetric stretching vibration peaks of P–O in the PO_4^{3-} groups. Vibration peak at 3570 cm^{-1} that attributed to the O–H was detected in S-HAp, and a quite weak vibration peak at 3567 cm^{-1} was detected for H-HAp (Sup Fig S3). Both XRD and FT-IR spectra data confirmed that S-HAp and H-HAp were roughly similar.

To study engraftment of the HAp crystals by VSMCs, HAp was dyed bright green by the fluorexon (Fig S1). As shown in Fig. 2E, both H-HAp and S-HAp were internalized into VSMCs after the HAp crystals were mixed with VSMCs for 24 h. Under EM, irregularly aggregated HAp crystals in different size were visible inside cytoplasm of VSMCs after mixing cells with HAp for 24 h (Fig. 2F). The images show that HAp crystals were gathered in the lysosomes, autophagosomes and autolysosomes.

3.3. Nano-HAp induced osteogenic differentiation of VSMCs and calcification deposition

To evaluate the effect of HAp on osteogenic differentiation of VSMCs, osteogenic marker proteins were examined. Expression of ALP, Runx2 and OPN was all increased significantly after VSMCs were treated with S-HAp (Fig. 3A) or H-HAp (Fig S4A) for 5 days as compared with those of the controls. The activity of ALP in VMSCs was also increased significantly after treated with HAp (Fig S4B). After VSMCs were treated with osteogenic medium (OM) or/and S-HAp ($VSMC^{S-HAp}$) for 14 days, significantly more calcium deposition in $VSMC^{S-HAp}$ was observed (Fig. 3B–D) as compared with VSMCs cultured in OM, whereas VSMCs

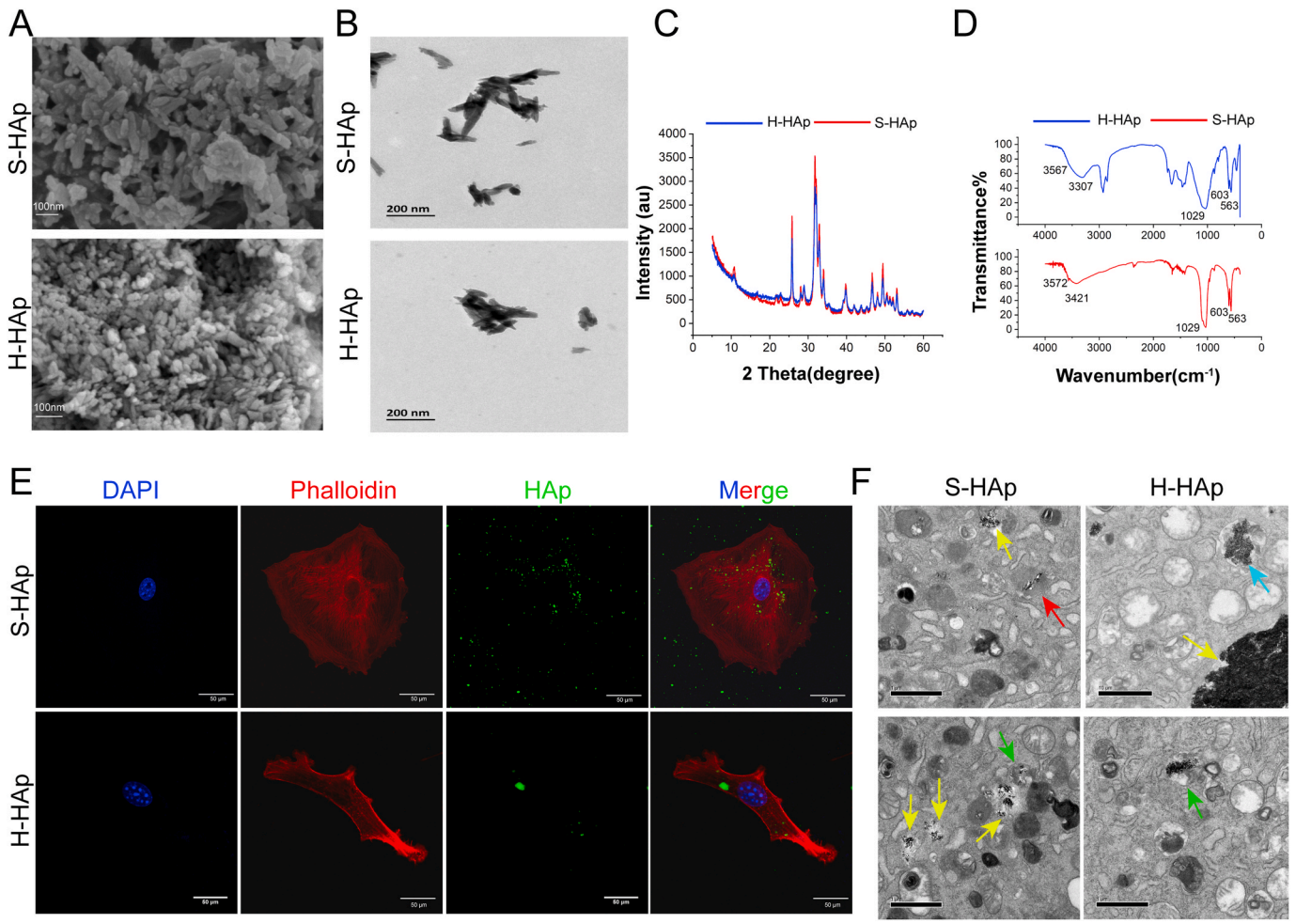

Fig. 2. Characterization and cellular uptake of HAp crystals. A) SEM of synthetic nHAp and human plaque derived HAp. Scal bar, 100 nm. B) TEM images of S-HAp and H-HAp. C) XRD pattern of S-HAp and H-HAp. D) FT-IR of S-HAp and H-HAp. E) Confocal microscopic images of VSMCs after mixed with 100 μg/mL fluorexon-labeled HAp for 24 h. Scale bar: 50 μm. F) TEM images of VSMCs after cultured with 100 μg/mL HAp for 24 h. Scale bar: 1 μm. Red arrow points lysosome, green arrows point autophagosomes, blue arrow points autolysosome and yellow arrows point aggregated HAp.

under normal medium showed no calcium deposition. VSMCs treated with both OM and S-HAp showed the synergistic effect on calcium deposition. Similar phenomena were also observed for VSMCs cultured with H-HAp (Fig S4C-E). These data indicated that both S-HAp and H-HAp crystals could induce calcification of VSMCs, and HAp crystals accelerated the development of calcification compared with the normal OM.

To further prove that nHAp can accelerate calcification, VSMCs were cultured with Tetracycline-HCl (TC) which produces fluorescence when combining with calcium ions. After VSMCs were cultured with TC under osteogenic medium (OM) for 5 days, very weak green fluorescence was detected (Fig. 3E). When VSMCs were cultured under nHAp and TC, the intensity of green fluorescence was significantly enhanced (Fig. 3E–F), confirming that progression of calcification of VSMCs was greatly accelerated by nHAp. In view of the fact that human samples are hard to obtain, we used S-HAp instead of H-HAp to conduct the following experiments on the basis of the above experiments.

3.4. Nano-HAp induced ectopic tissue calcification in vivo

To investigate whether nHAp can directly contribute to mineralization of ECM in vivo, Matrigel mixed with VSMCs or/and S-HAp were subcutaneously implanted into the dorsum of C57BL/6 mice (Fig. 4A). Greater calcification was detected using micro-CT at the region injected with both VSMCs and S-HAp as compared to that with S-HAp only (Fig. 4B–C) after implantation for 1 month. No calcification was observed at the site injected with VMSCs only. Likewise, the calcium content in the recovered subcutaneous tissues with both VSMCs and S-HAp was the highest among 3 groups (Fig. 4C). Calcific deposits and cells were identified in the recovered subcutaneous tissues (Fig S5). Most of the cells in the recovered tissues with VSMCs and S-HAp were GFP positive, indicating that they were the originally implanted VSMCs, and they were strong positive for osteogenic marker Runx2; whereas in the tissue with VSMCs only, significantly less Runx2 was detected in the GFP^+ VSMCs (Fig. 4D). As expected, neither GFP^+ cells nor Runx2 were detected in the recovered tissues with S-HAp only. These results confirmed that nHAp possessed the ability to induce osteogenic differentiation of VSMCs and ectopic matrix mineralization in vivo.

To further confirm the effect of nHAp on vessel calcification, we applied S-HAp to the out surface of mouse abdominal aorta whose adventitia was torn off. Calcification dots on the aorta being applied with either S-HAp or $CaCl_2$ were detected by enhanced micro-CT (Fig. 4F) or directly viewed under stereomicroscope (Fig. 4G) 14 days after the surgery, while application of control NaCl to aorta resulted in no calcium deposits, which was further confirmed by the von Kossa staining of the vessels (Fig. 4G). Significantly more Runx2 was co-localized with SMCs marker α-SMA on the aorta treated with S-HAp or $CaCl_2$ as compared to that treated with NaCl (Fig. 4I). These results indicate that nHAp could induce osteogenic differentiation of SMCs and vascular calcification in vivo.

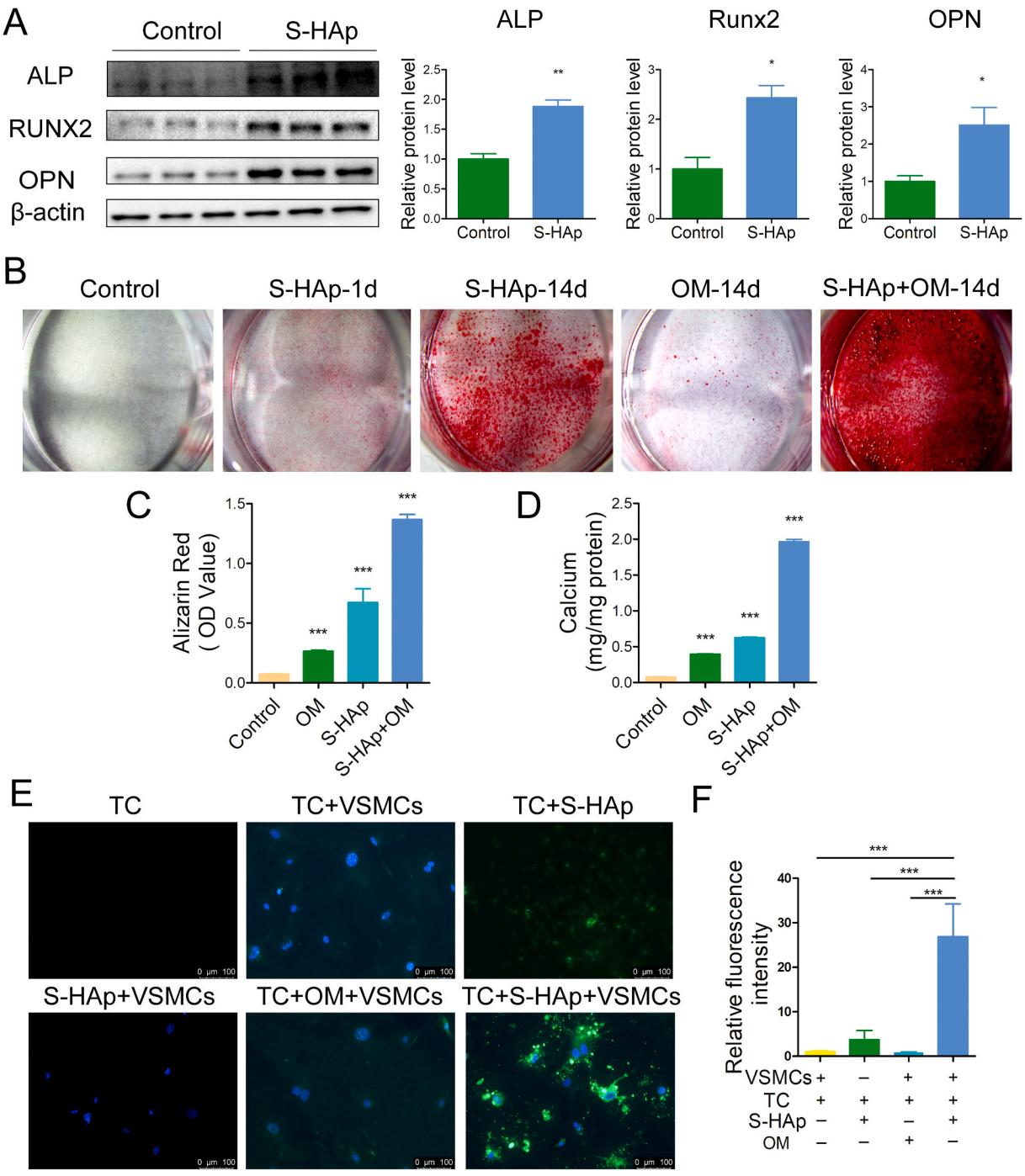

Fig. 3. nHAp induced osteogenic transdifferentiation of VSMCs and calcification deposition. VSMCs were mixed with 100 μg/mL S-HAp for 1 day and then washed with PBS to remove HAp and further cultured for specified days. A) Protein expression of ALP, RUNX2 and OPN in VSMCs 5 days post S-HAp treatment was analyzed by western blot. The bar graphs show quantification of ALP, Runx2 and OPN expression. B) VSMCs were stained for mineralization by Alizarin red to show calcium deposition after 14 days' treatment. C) Quantification of Alizarin Red extracted from the cultures in B to represent the amount of calcium. D) Total calcium in the dishes was quantified. E) VSMCs were treated with 40 μg/mL tetracycline-HCl (TC) and 100 μg/mL S-HAp or OM for 5 days, then washed with PBS and stained with DAPI (blue). Representative fluorescent images showing the newly formed calcium phosphate crystals (green). The TC group and the S-HAp + VSMCs group are represented as negative control. F) Quantification of the green fluorescence intensity. Data are expressed as the mean ± SD (*$p < 0.05$, **$p < 0.01$, ***$p < 0.001$).

3.5. Nano-HAp induced accumulation of autophagosomes in VSMCs

Under TEM, we observed increased number of double-membrane autophagosomes in $VSMC^{HAp}$ (Fig. 5A and Fig S6A) as compared to the control cells, indicating that internalization of HAp could cause the accumulation of autophagic organelles. Indeed, almost 4-fold more LC3, a classical marker for autophagy, was detected on the calcified artery than that on the control (Fig. 5B). More puncta formation of endogenous LC3 was observed in $VSMC^{S-HAp}$, while less and evenly dispersed LC3 throughout the cytoplasm was seen in the control cells (Fig. 5C). Furthermore, significantly higher LC3-II was detected in $VSMC^{HAp}$ than the untreated controls (Fig 5D, and Fig S6B), indicating that HAp stimulated the conversion of cytoplasmic LC3-I to membrane-conjugated LC3-II. Taken together, these data demonstrate that both

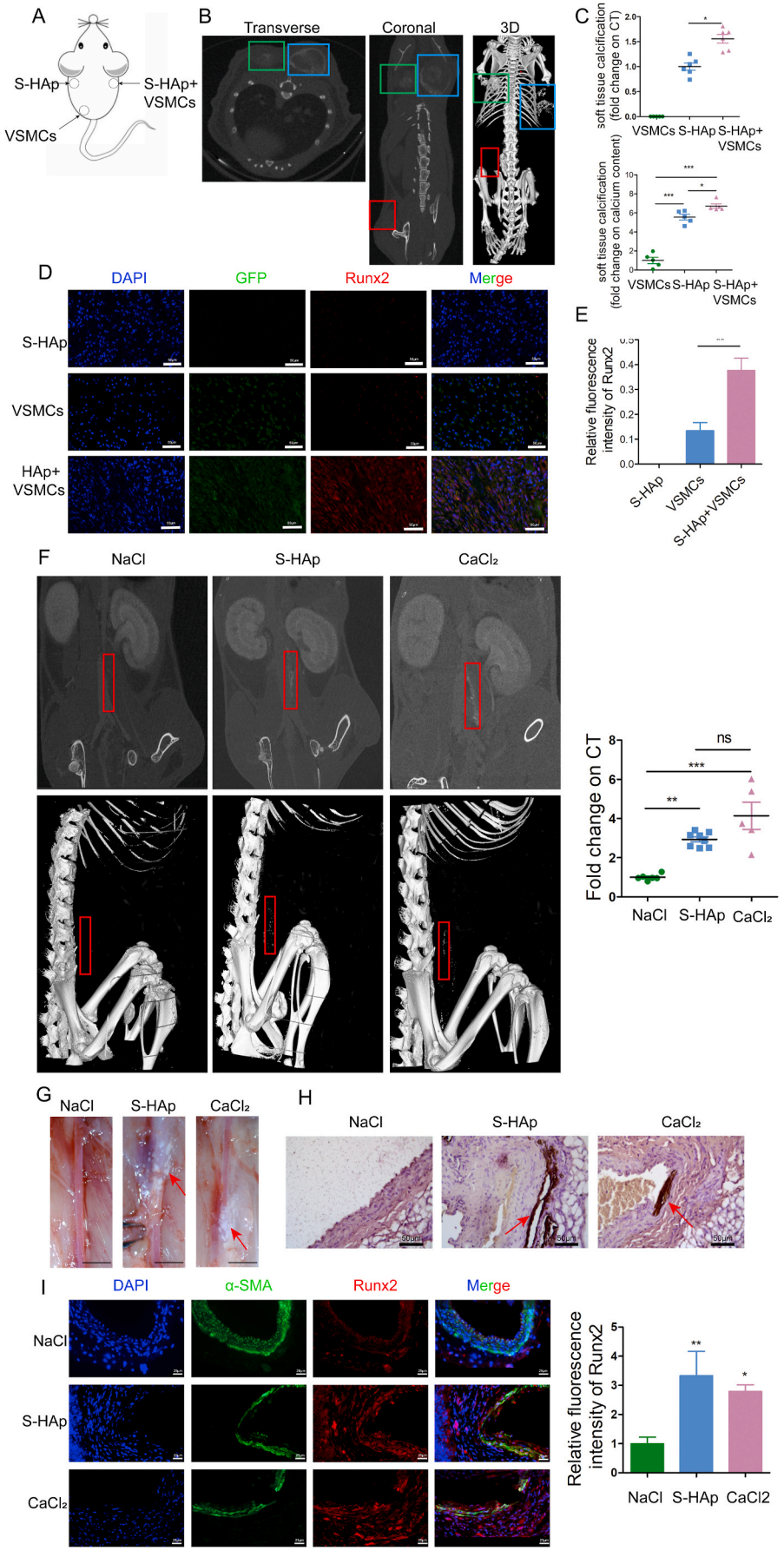

Fig. 4. Nano-HAp induced ectopic tissue calcification in vivo. A) Ectopic tissue calcification experimental strategy showing that Matrigels mixed with 1) GFP transduced VSMCs, 2) S-HAp, 3) GFP transduced VSMC plus S-HAp, were separately injected into 3 subcutaneous pockets fashioned on the dorsum of mice. B) CT scan to detect calcification in the Matrigels after implantation for 1 month. Robust calcification was detected in the areas injected with Matrigels containing S-HAp, while the calcium content was higher in the region with VSMCs (blue box) than that without cells (green box). No calcification was observed in the region of matrigel with VSMCs only (red box). C) Calcification was quantified as a fold change in comparison with the region with VSMCs only. Data are expressed as mean ± SD, *p < 0.05. D) Immunofluorescent staining of dissected subcutaneous tissue detected the implanted GFP^+ cells and expression of Runx2. Scale bar: 50 μm. E) The bar graph shows Runx2 expression. N = 6. Data are expressed as mean ± SD, *p < 0.05. F) Enhanced CT scan detects calcification on abdominal aorta in mice 14-day after adventitia was torn off, and S-HAp, or $CaCl_2$ (a positive control), or NaCl (a negative control) were applied to the out surface of the mouse abdominal aorta. Representative images of CT scan showing calcium deposition on the aorta. Red boxes are the position of aorta with calcification. The right panel shows quantification of calcification on the aorta from the CT scan. G) Representative images of the aorta under stereomicroscope to show the calcium deposits (white). Scale bar: 200 px. H) Representative images of the aorta sections stained with von Kossa to detect calcium deposit (brown). I) Representative images of the aorta sections after immunofluorescent staining for Runx2 and α-SMA. Scale bar: 25 μm. The right panel shows quantification of Runx2 expression on the vessel. N = 6. Data are expressed as mean ± SD, *p < 0.05.

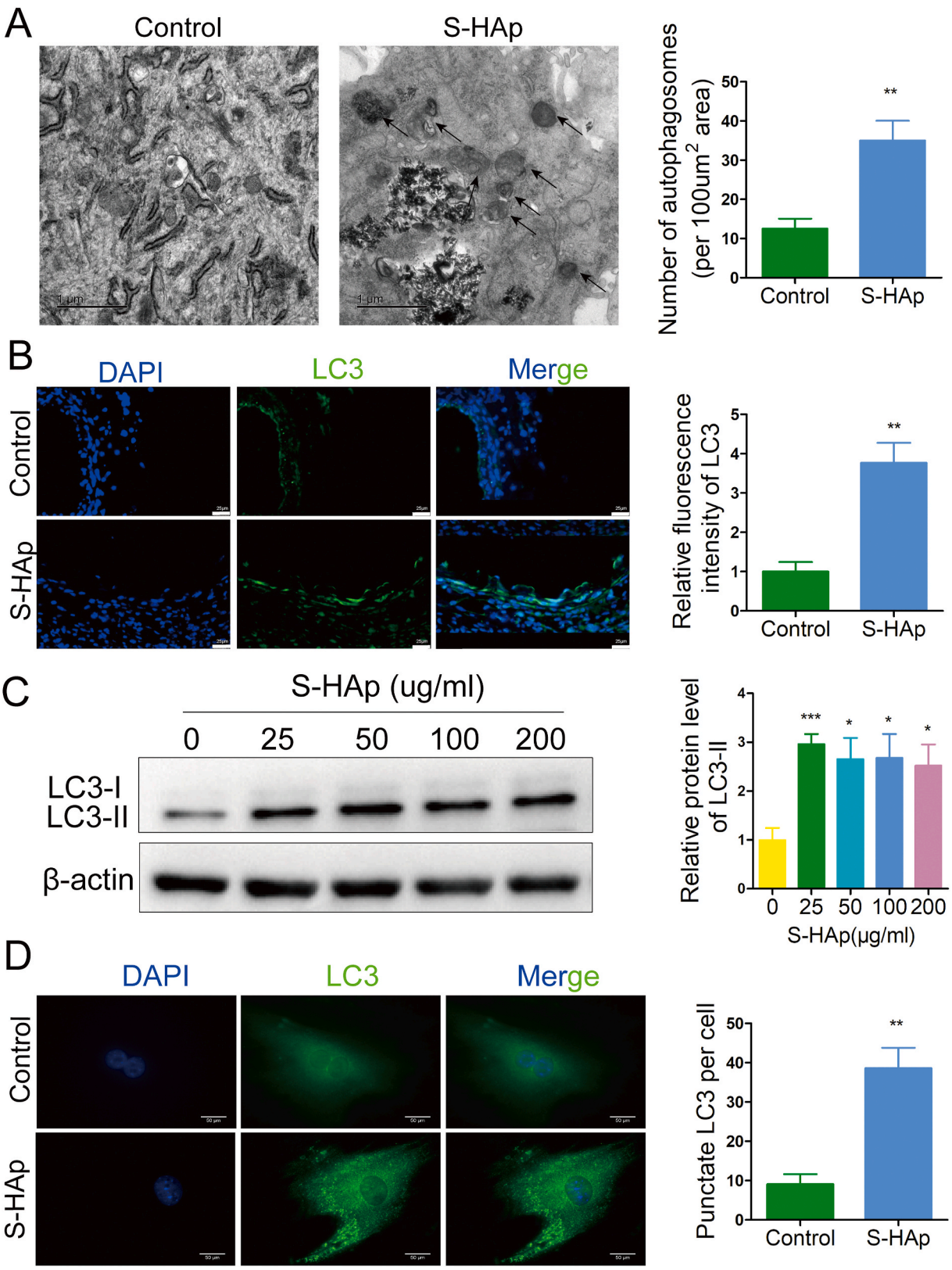

Fig. 5. Nano-HAp induced accumulation of autophagosomes in VSMCs. A) Autophagic vacuoles in cells with or without 100 μg/mL S-HAp treatment were observed by TEM. The arrow indicates autophagic vacuoles. Scale bar: 1 μm. Data are presented as mean ± SD. B) Representative images of immunofluorescent staining for LC3 on the recovered aorta whose outside has been applied with NaCl or S-HAp. Expression of LC3 was quantified by measuring the relative fluorescence intensity from 10 sections. Scale bar: 25 μm. C) VSMCs were treated with different concentrations of S-HAp for 24 h, and the cellular LC3 expression levels were detected by western blot. The relative LC3-II protein level was quantified in the bar graph. D) Images of immunofluorescence analysis show the LC3 distribution patterns in the control and crystals-treated cells. Scale bar: 50 μm. The number of punctate LC3 per cell were quantified. Data are expressed as mean ± SD. (*$p < 0.05$).

types of HAp crystals induced accumulation of autophagosomes in VSMCs.

The classical pathway of autophagy induction involves inhibition of mTOR, usually induced by energy reduction. We found that S-HAp did not alter the phosphorylation of either mTOR or AMPK (Fig S7A), suggesting that S-HAp stimulates formation of autophagosomes through a pathway different from starvation-induced mTOR inhibition. Rapamycin, an inhibitor of mTOR, which induces autophagy, additively increased LC3-II level in VSMC^{S-HAp} (Fig S7B), further confirming that S-HAp-stimulated production of autophagosomes involves a pathway independent of mTOR inhibition.

3.6. Nano-HAp inhibited autophagic degradation without effecting fusion of autophagosome with lysosome

Accumulation of autophagosomes could be a result of autophagy induction or blockage of autophagosome clearance which involves fusion of autophagosomes with lysosomes and thereafter degradation of

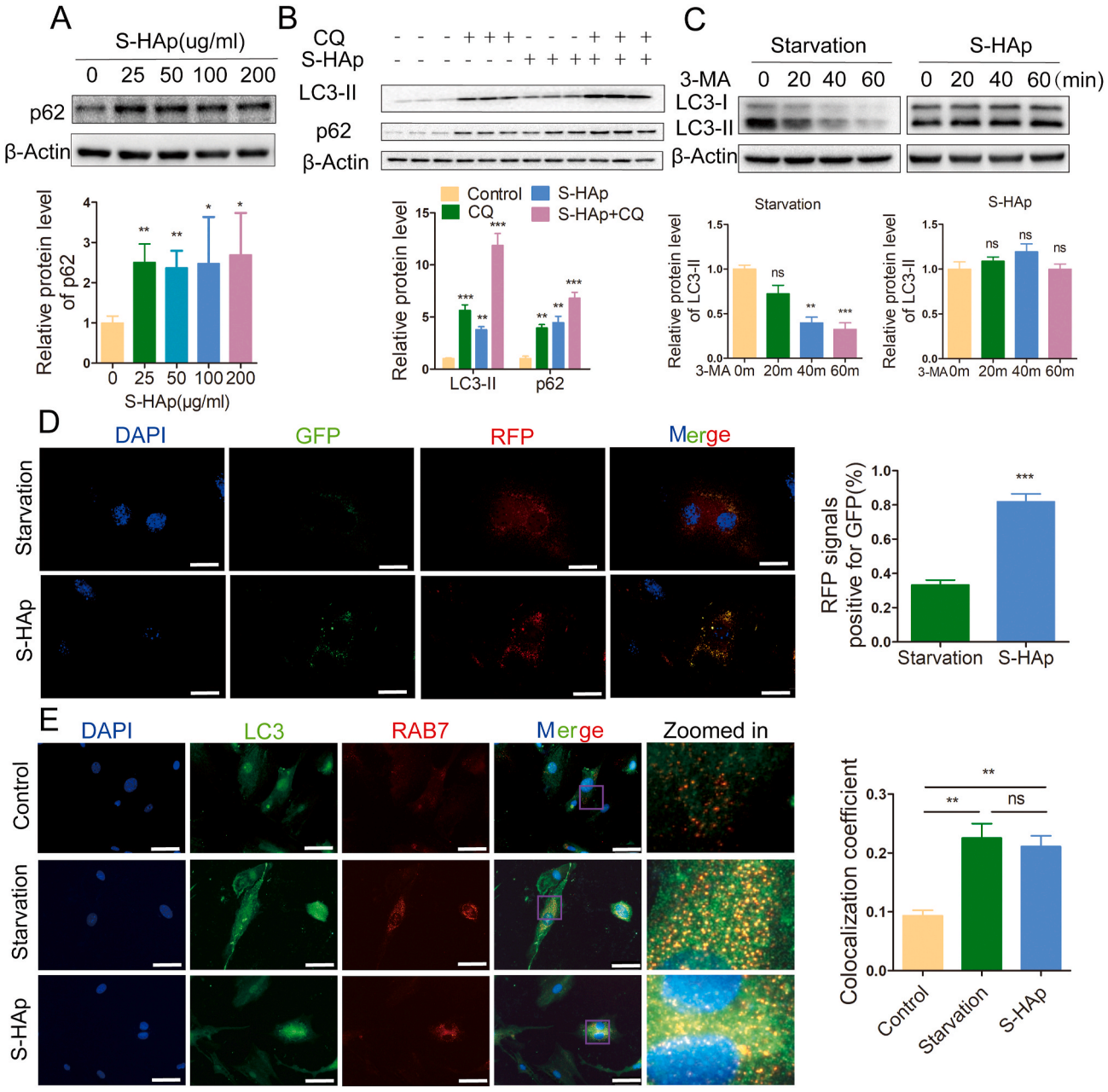

Fig. 6. Nano-HAp inhibited autophagic degradation. A) Western blot analysis of p62 in VSMC^{S-HAp} at the specified concentration of S-HAp for 24 h. The relative p62 protein level was quantified in the bar graph. B) Western blot analysis of p62 and LC3-II in VSMCs that were treated with S-HAp for 24 h, with or without CQ (10 μmol/L) cotreatment for the last 3 h. The relative protein levels were quantified in the bar graph. C) Western blot analysis of LC3-II in VSMCs that were treated with S-HAp at 100 μg/mL for 24 h or starvation medium, and then treated with 1 mM of 3-MA. The relative LC3B-II protein level was quantified in the bar graph. D) Representative immunofluorescence images show LC3 in VSMCs that were transduced with mRFP-GFP-LC3 adenoviral vector and cultured under starvation condition for 24 h or S-HAp (100 μg/mL) treatment. GFP fluorescence is pH sensitive while RFP is not. Starvation-induced autophagy flux caused the fusion of autophagosome with lysosome, which resulted in quenching GFP fluorescence signal; when autophagy flux was blocked by S-HAp, much less GFP fluorescence signal was quenched. Relative GFP fluorescence intensity over RFP was quantified in the bar graph. Scale bars: 50 μm. E) Immunostaining with antibodies against Rab7 and LC3. Cells were starved, or treated with or without HAp for 24 h. Scale bar: 50 μm. The colocalization coefficient of RAB7 and LC3 was represented as percentage of punctate signals of LC3 that were positive for RAB7.

the resulted autolysosomes [28]. S-HAp did not increase the mRNA of LC3 (Fig S8A), indicating that HAp-induced increase in LC3 was not due to enhanced LC3 expression for more autophagosome formation.

Protein sequestosome 1 (p62) is a selective autophagic receptor that is incorporated into autophagosomes and preferentially degraded along with other substrates by lysosomal hydrolysis. Level of p62 protein was increased after VSMCs were treated with S-HAp or H-HAp (Fig. 6A, and Fig S6B). Immunostaining showed more cytoplasmic p62 proteins were assembled into aggregates in VSMC^{S-HAp} (Fig S9A). Such effect of HAp on accumulation of p62 was not due to more p62 expression as its mRNA level was not different from that in the untreated cells (Fig S8B). When chloroquine (CQ), an inhibitor of autophagosome-lysosome fusion, was added into the culture, both LC3II and p62 were additively elevated (Fig. 6B). These data indicate that nHAp could inhibit the degradation of p62 by blockade of the autophagy flux. Such phenomenon was also confirmed in vivo. Levels of both LC3-II and p62 were higher in the S-HAp-treated aorta than that of NaCl-treated aorta (Fig S10).

When 3-methyladenine (3-MA), an inhibitor of autophagosome synthesis, was added to the starved cells, LC3-II was significantly reduced; however, such 3-MA mediated reduction of LC3-II did not occur in VSMC^{S-HAp} (Fig. 6C), also suggesting that nHAp blocks autophagosome degradation.

Autophagic flux was further examined by transferring mRFP-GFP-LC3 fused genes in adenoviral vector. Under starvation, autophagy was enhanced, fusion of autophagosomes with lysosomes quenched the GFP signal (Fig. 6D), thanks to the quenching of GFP fluorescence (but not RFP) in acidic compartments. However, when the cells were cultured with S-HAp, quenching of GFP fluorescence was significantly reduced (Fig. 6D), confirming that S-HAp blocks autophagic flux and autophagic degradation. This could be caused by two reasons: one is the fusion of autophagosome and lysosome is blocked, and the other one is the lysosome function is impaired.

To investigate the formation of autolysosomes, co-localization of autophagosomal LC3 with lysosome-anchored Ras-related protein 7 (Rab7), a GTPase, was examined to implicate the fusion of autophagosome with lysosome. LC3 was poorly colocalized with Rab7 in control VSMCs, while starvation enhanced the colocalization, demonstrating the formation of autolysosome (Fig. 6E). Nano-HAp treatment of VSMCs resulted in a similar colocalization of LC3 and Rab7 as that of starved cells, indicating that the formation of autolysosomes was not affected by nHAp. This was further confirmed by colocalization of LC3 with the lysosomal associated membrane protein 1 (LAMP1) (Fig S11).

3.7. Nano-HAp impaired lysosomal degradation through inhibiting lysosomal acidification

Autophagy is a degradation process in cooperation with lysosomes. Since nHAp does not affect the fusion of autophagosome with lysosome, we then examined the function of lysosomes. The expression of early endosomal antigen 1 (EEA1), which is a marker of endosome [29], and LAMP1 both increased in VSMCs after S-HAp treatment (Fig S13), indicating that S-HAp may enter VSMCs through endosome/lysosome pathway. Entry of S-HAp into lysosome was observed after mixing S-HAp with VSMCs for 24 h (Fig. 7A), which could impair the function of lysosomes. We then evaluated the ability of lysosomal degradation using a degradation assay of epidermal growth factor receptor (EGFR). EGFR was localized primarily on cell surface and was internalized and clustered into puncta after binding with its ligand EGF. Clustered EGFR was observed at 1 h post EGF treatment, and then was degraded later in the control VSMCs (Fig. 7B). However, such EGFR puncta were retained in VSMC^{S-HAp}, indicating weakened lysosomal proteolysis. This was further confirmed by western blot analysis showing that total cellular EGFR was retained in VSMC^{S-HAp} while a timely reduction of EGFR was observed in the control cells (Fig. 7C). These data indicate that nHAp impairs lysosomal degradation capacity.

Next, we examined the acidification ability of lysosomes since acidification is essential for the maturation and activation of most lysosomal enzymes. Acridine orange (AO) staining was used to assess the acidification of lysosomes. In cytosol, AO exists in nonprotonated monomeric form and emits green fluorescence. When it enters acidic lysosomes, the protonated form of AO aggregates and fluoresces bright red. As shown in Fig. 7D, red fluorescence of AO was dramatically reduced in VSMC^{S-HAp} as compared with that in control cells, indicating a reduced acidified-compartments in VSMC^{S-HAp}.

In addition, more pre-matured cathepsin D (CTSD) at 43-kDa, a lysosomal protease, and less matured CTSD were detected in VSMC^{S-HAp} in comparison with that in the control cells (Fig. 7E), indicating a suppression of the conversion from pre-matured to matured form.

To understand the alteration of acidification and subsequent lysosome immaturation in VSMC^{HAp}, the subcellular localization of V-ATPase, an ATP-driven proton pump that imports protons into lysosomal lumen for the acidification of the compartment was examined. V1D subunit of V-ATPase was colocalized strongly with lysosome membrane protein LAMP1 in the control cells, while this colocalization was disrupted in VSMC^{S-HAp} (Fig. 7F), suggesting a failure in the targeting of V-ATPase V1D subunit to lysosomes in VSMC^{S-HAp}. These results demonstrated that nHAp impairs lysosomal acidification.

3.8. HAp-induced calcification was caused by autophagy dysfunction in VSMCs

To investigate the relationship between autophagy and calcification, we utilized autophagy stimulator rapamycin (RAPA) and autophagy inhibitor chloroquine (CQ) (Fig S12). RAPA and CQ themselves did not affect calcification in VSMCs (Fig. 8A). When S-HAp was added along with either RAPA or CQ, stronger Alizarin red staining with more calcium deposition in VSMCs was detected (Fig. 8A), suggesting that both RAPA and CQ enhanced the calcification induced by S-HAp.

To confirm that the blockage of autophagy flux accounts for nHAp-induced calcification, cAMP was used to restore lysosomal acidification. Both LC3-II and p62 levels in S-HAp-treated VSMCs were significantly reduced by cAMP (Fig. 8C–D), suggesting that the reacidification of lysosomes enhances autophagic flux and promotes autophagic degradation. After cAMP treatment, calcification of S-HAp-treated cells were significantly attenuated (Fig. 8E–F). Collectively, the data above indicated that S-HAp-induced calcification is a result of impaired autophagic degradation.

3.9. Nano-HAp promoted release of exosomes containing LC3 and LAMP1

Since exosome budding off plasma membrane has been proposed as a mechanism of calcification, and the interplay of autophagy and exosomal secretion was reported recently, we postulated that the accumulated autophagosomes and autolysosomes can be converted into exosomes and then secreted out of cells to lead calcification. To confirm that, exosomes (Exos) were purified from the conditioned medium of VSMCs and characterized (Fig S14). More Exos (18.8 ± 0.6 μg/10^7 cells) were harvested from VSMC^{S-HAp} than that from VSMCs (7.5 ± 0.5 μg/10^7 cells) (Fig. 9A). There was more exosome specific marker CD9 as well as autolysosome-associated LC3 and LAMP1 proteins in Exos from VSMC^{S-HAp} than VSMCs (Fig. 9B). Calcium content in Exos from VSMC^{S-HAp} was significantly higher (139.7 ± 1.6 ng/10^7 cells) than that from VSMCs (64.4 ± 1.6 ng/10^7 cells) (Fig. 9C). When GW4869, an inhibitor of neutral sphingomyelinase (nSMase), was added to the culture to block Exos release, significantly less Exos were harvested from VSMC^{S-HAp}. Exosome specific protein CD9, and autolysosome-associated LC3 and LAMP1 were correlatively reduced in Exos from VSMC^{S-HAp} treated with GW4869 (Fig. 9D–E), as well as the calcium content (Fig. 9F). Accordingly, when VSMC were treated with S-HAp in the presence of GW4869, calcium deposits were significantly reduced as compared with VSMC^{S-HAp} (Fig. 9G).

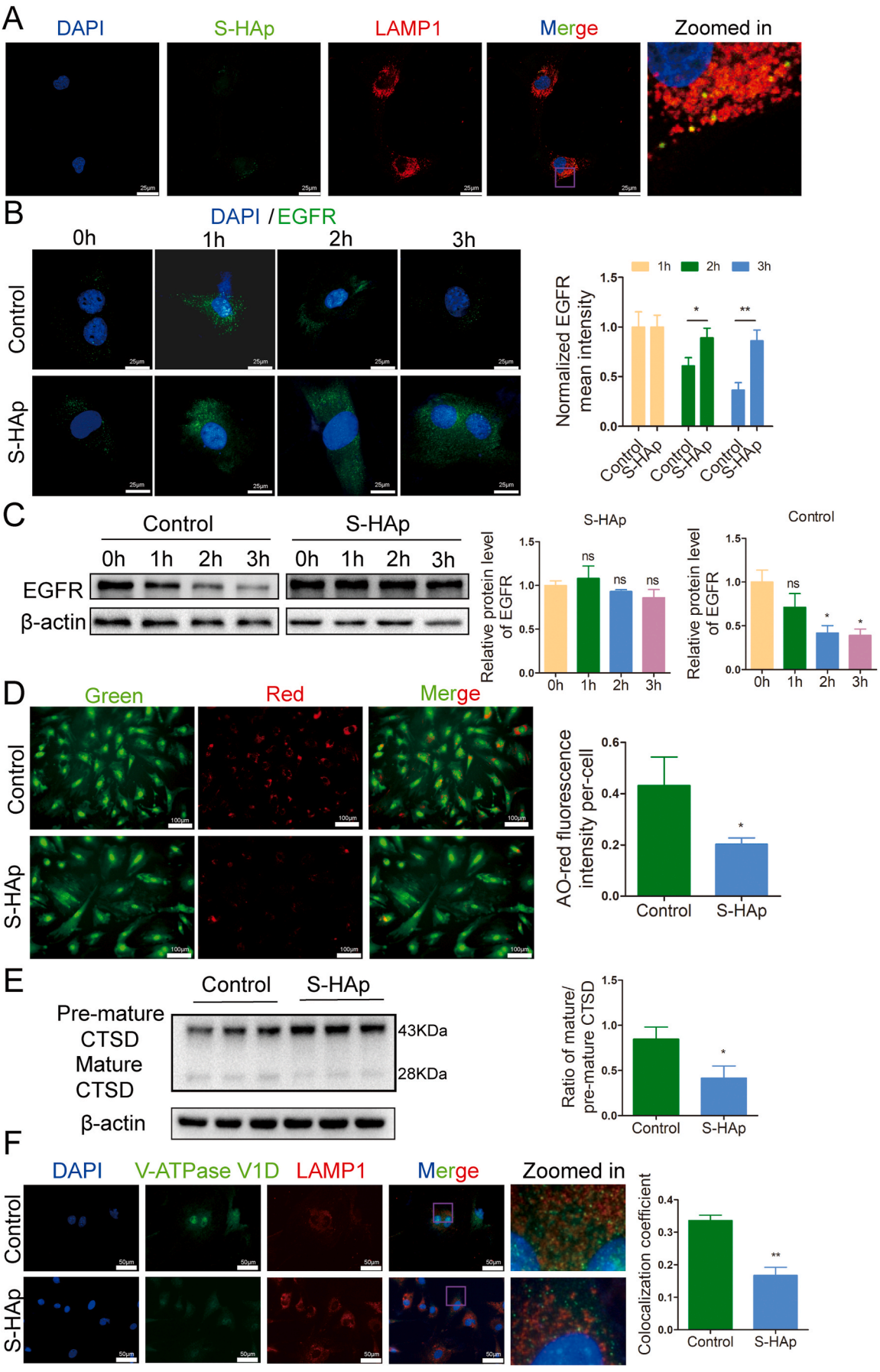

(caption on next page)

Fig. 7. Nano-HAp impaired lysosomal degradative capacity and inhibited lysosomal acidification. A) Representative confocal immunofluorescence images show colocalization of S-HAp and LAMP1 in VSMCs. The cells were treated with 100 μg/mL fluorexon labeled S-HAp for 24 h, and then stained with LAMP1 antibody. The yellow dots represent the colocalization of S-HAp and the lysosome. B) VSMCs were treated with 100 μg/mL of S-HAp for 24 h, and then treated with 50 ng/mL EGF for 0, 1, 2 and 3 h which was removed after the specified time. The cells were fixed and immunostained with anti-EGFR antibody. Scale bars: 25 μm. Quantitative analysis of EGFR was performed by normalization to the green fluorescence intensity of cells with EGF treatment for 1 h. C) Western blot analysis of EGFR protein in the cells treated as in (A) and their quantification. D) VSMCs treated with or without S-HAp were labeled with acridine orange (AO). Red fluorescence of AO staining per cell was quantified. Scale bar: 100 μm. E) Western blot analysis of CTSD protein in VSMCs which had been treated with 100 μg/mL nHAp for 24 h. The ratio of mature-CTSD to premature-CTSD was quantified in the bar graph. F) Representative immunofluorescence images show V-ATPase V1D and LAMP1 in VSMCs which were treated with or without 100 μg/mL S-HAp for 24 h, and then stained with antibodies against V-ATPase V1D and LAMP1. The colocalization coefficients of V-ATPase V1D and LAMP1 were quantified as percentage of punctate signals of V-ATPase V1D that were positive for LAMP1. Data are presented as mean ± SD (*$p < 0.05$).

To confirm that undissolved S-HAp could be carried out of the cells via Exos after they were internalized into VSMCs, fluorexon-labeled S-HAp were cultured with VSMCs. Fluorescence signal was detected in the Exos purified from the conditional medium of $VSMC^{S-HAp}$. These data suggest that nHAp promoted release of Exos from VSMCs, and these Exos were at least partly originated from the accumulated autophagic vesicles which were resulted from the blockage of autophagy flux by nHAp (Fig. 9H).

4. Discussion

In this study, we demonstrated nHAp existed in calcified artery, and observed internalization of nHAp into VSMC. Nano-HAp stimulated osteogenic differentiation and accelerated mineralization of VSMCs in vitro, and enhanced calcium deposits in artery in vivo. Such effect of nHAp on promoting VC was through altering lysosomal acidification and impairing the degradation function of thereafter formed autolysosomes. We first discovered that the blockage of autophagy flux by nHAp resulted in accumulation of autophagosomes and autolysosomes in VSMCs, which were turned into more calcium-containing exosomes released into ECM (Fig S15).

Nano-HAp could be both a result and cause of vascular calcification processes. HAp crystals had been isolated from human carotid atherosclerotic plaques [25] and suggested to contribute to early osteoblastic transdifferentiation of cardiovascular cells [30]. Here we detected the deposition of nano-crystalline in human calcified aorta, existence of nHAp in VSMC, and onset expression of Runx2 (Fig. 1). We demonstrated that synthetic HAp and human-derived crystals were similar in morphology and characteristics (Fig. 2). The results were consistent with previous results that the contents of vascular calcification are composed of highly crystalline hydroxyapatite [30]. Therefore, XRD peak intensity of H-HAp is similar with that of S-HAp. As reported, vascular apatitic mineral contains carbonate and magnesium impurities [3], which is consistent with our EDS results (Fig S2B). Because the crystals from vascular atherosclerotic plaque contained some organic contents like fatty acids, FT-IR results may be inconsistent between H-HAp and S-HAp, resulting in two strong organic peaks at 2900 cm^{-1} and 3300 cm^{-1}. This also makes the OH^- peak of H-HAp at 3567 cm^{-1} weak (Fig. 2B, Sup Fig S3).

Both S-HAp and H-HAp can accelerate calcium deposition of VSMCs via blockage of autophagy flux and accumulation of autophagic vacuoles. Studies have shown that nHAp promoted osteogenic differentiation of mesenchymal stem cells (MSCs) and osteoblasts with the increased expression of Runx2, OCN and ALP [31–35]. Such effect of nHAp on mineral deposition has been translated into clinical use of nHAp for bone repair [36]. The effect of HAp on VSMCs had also been studied, and upregulation of BMP-2 and OPN gene expression was found in VSMCs after treated with Pi-induced nanocrystals [37]. Calcifying nanoparticles (CNPs) extracted from human serum was found to induce accumulation of apoptotic bodies and accelerate vascular calcification [5]. CNPs were detectable in calcific but not healthy human arteries. They could propagate and induce mineral deposition in vitro with sufficient Pi [4,38]. However, these studies are lack in clinical evidence and short in mechanism and in vivo experiment. Our study confirmed that nano-sized HAp existed in calcified aorta and can be internalized into VSMC. The EDS data showed the nano-sized crystals contained calcium and phosphorus, and the ratio of Ca/P was about 1.47, which was consistent with the results of Sergio Bertazzo et al. [30] and Alexandra E. Ewence et al. [25]. Both S-HAp and H-HAp can elevate the expression of Runx2 and OPN and the activity of ALP (Fig 3A and Fig S4A-B), and expedited calcium deposition in VSMCs (Fig. 3B). With additional HAp supplied in the osteogenic medium, OM-induced calcification was significantly enhanced (Fig. 3B), which is supported by the recently published report [6]. In addition, we also demonstrated that nHAp greatly stimulated new calcium deposition in VSMCs, and accelerates the development of calcification (Fig. 3E–F). The acceleration effect of nHAp on the development of calcification could be two parts. One is that the originally formed nHAp promoted calcium deposition of VSMCs by blockage of autophagic flux; and the other is that nHAp with "Ca + Pi" had a synergistic effect, resulted in a faster rate of calcification than that of the normal OM.

To confirm the effect of nHAp on calcification in vivo, S-HAp was implanted underneath the skin or outside of aorta. Implantation of S-HAp directly induced calcium deposition (Fig. 4A–C). When nHAp was implanted along with VSMCs, more calcium deposition was observed (Fig. 4C) and the implanted VSMCs were differentiated in osteogenic phenotypes with more Runx2 expression (Fig. 4D), demonstrating that nHAp can induce VSMCs osteogenic differentiation in soft tissue. When nHAp was applied to the outside of abdominal aorta, significant calcification was observed in the vascular wall after 2 weeks (Fig. 4F–G). According to previous studies, both $CaCl_2$ and $CaPO_4$ could induce calcification deposition on artery [39]. Here, we employed $CaCl_2$ as a positive control which indeed showed substantial calcification in artery (Fig. 4F–H). This is the first time to demonstrate that nano-sized HAp induced direct vascular calcification in vivo.

Autophagy is a key regulator of cellular metabolism and homeostasis. Emerging evidence has demonstrated that autophagy plays an important role in vascular calcification. It has been documented that atorvastatin protected VSMCs from TGF-β1-stimulated calcification by inducing autophagy through suppression of the β-catenin pathway [9]. Another study demonstrated that estrogen inhibited osteoblastic differentiation of VSMCs in vitro and prevented arterial calcification in vivo by promoting autophagy through the ERα signaling pathway [40]. These studies demonstrated a protective role of autophagy in vascular calcification [10]. Recent investigations point to the critical and defensive role of autophagy in the behavioral function of vascular cells against different insults [41], which was mainly focused on the death and phenotypic change of VSMCs without precise mechanism. Here, we found that nHAp was internalized by VSMCs (Fig. 2E–F) and caused accumulation of autophagosomes (Fig 5A & S6A). It has great clinical significance to figure out whether blockage of autophagy flux contributes to nHAp-induced calcification.

In our study, we found that both S-HAp and H-HAp crystals increased intracellular autophagosomes (Fig 5A, and Fig S6A) and elevated autophagic cargo proteins, including LC3-II and p62 in the VSMCs (Figs. 5C and 6A and Fig S6B), and the process is mTOR-independent. This was due to blockage of autophagic flux by nHAp-induced dysfunction of autolysosome degradation. The underlying mechanism

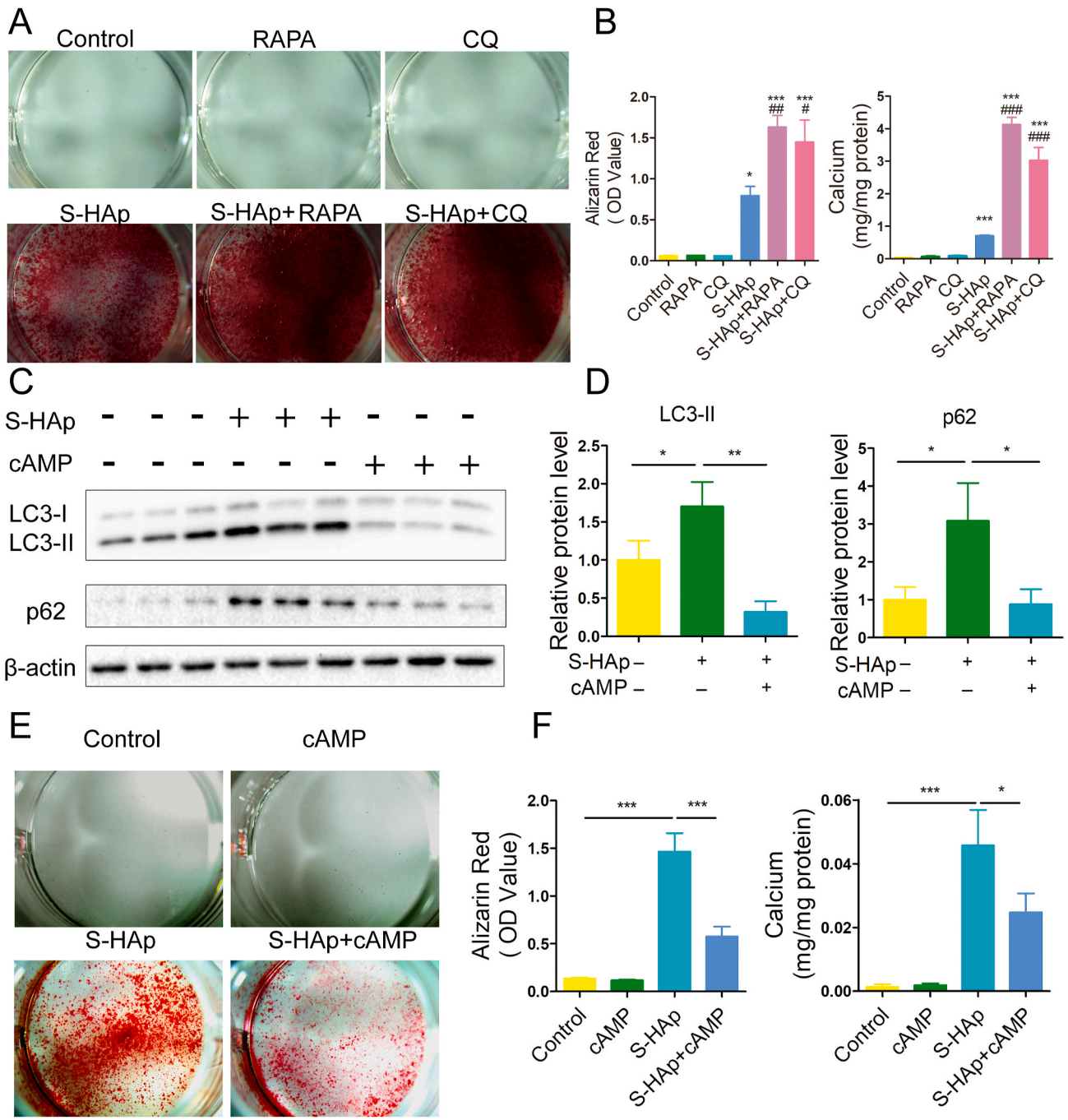

Fig. 8. Autophgy dysfunction of VSMCs was related with calcification induced by nHAp. A) Alizarin red staining of VSMCs that were pretreated for 3 days with RAPA or CQ followed by addition of S-HAp for 14 days. B) Alizarin red and calcium content on the cells were quantified. Data are expressed as the mean ± SD. (*vs control, #vs S-HAp. $*p < 0\ 05$, $***p < 0.001$, $\#p < 0.05$, $\#\#\#p < 0.001$). C) VSMCs were exposed to S-HAp at 100 μg/mL for 24h, or with cAMP cocktail. The expression of corresponding proteins was detected by western blot. D) The statistics for relative LC3-II and p62 protein level. E) VSMCs were treated with 100 μg/mL S-HAp, or cAMP cocktail, or both for 14 days. Alizarin red staining was used to evaluate the calcification. F) Alizarin red and calcium content on the cells were quantified. Data are expressed as the mean ± SD, $*p < 0\ 05$.

was further elucidated that acidification of lysosome was inhibited by S-HAp (Fig. 7D). However, Wang, et al. proved that nHAp modulated osteoblast differentiation by mediating autophagy via mTOR signaling pathway [42], which is inconsistent with our results. Our data suggest an involvement of an inhibitory effect of nHAp on the late stage of autophagy. This conclusion was supported from 3 lines of evidence. First, nHAp had an additive effect on rapamycin-induced production of LC3-II (Fig S7B); second, nHAp arrested the degradation of LC3 and p62, the selective autophagy substrates (Fig. 6); third, nHAp prevented the maturation of lysosomes, leading to lysosomal dysfunction (Fig. 7). Our results first demonstrate that nHAp-induced autophagy dysfunction by lysosomal impairment resulted in vascular calcification. Lysosomal impairment could be a general toxic mechanism of nanoparticles to cells [43,44]. Previous studies testified lysosomal disfunction exacerbates vascular calcification [45,46]. This provides evidence to focus on lysosomal function in our study. Mechanism underlining nHAp-induced dysfunction of autolysosome degradation was further studied by analyzing lysosomal acidification. We found that nHAp impaired lysosome maturation by inhibiting lysosomal acidification without disturbing fusion between autophagosome and lysosome (Fig. 6E). Degradation

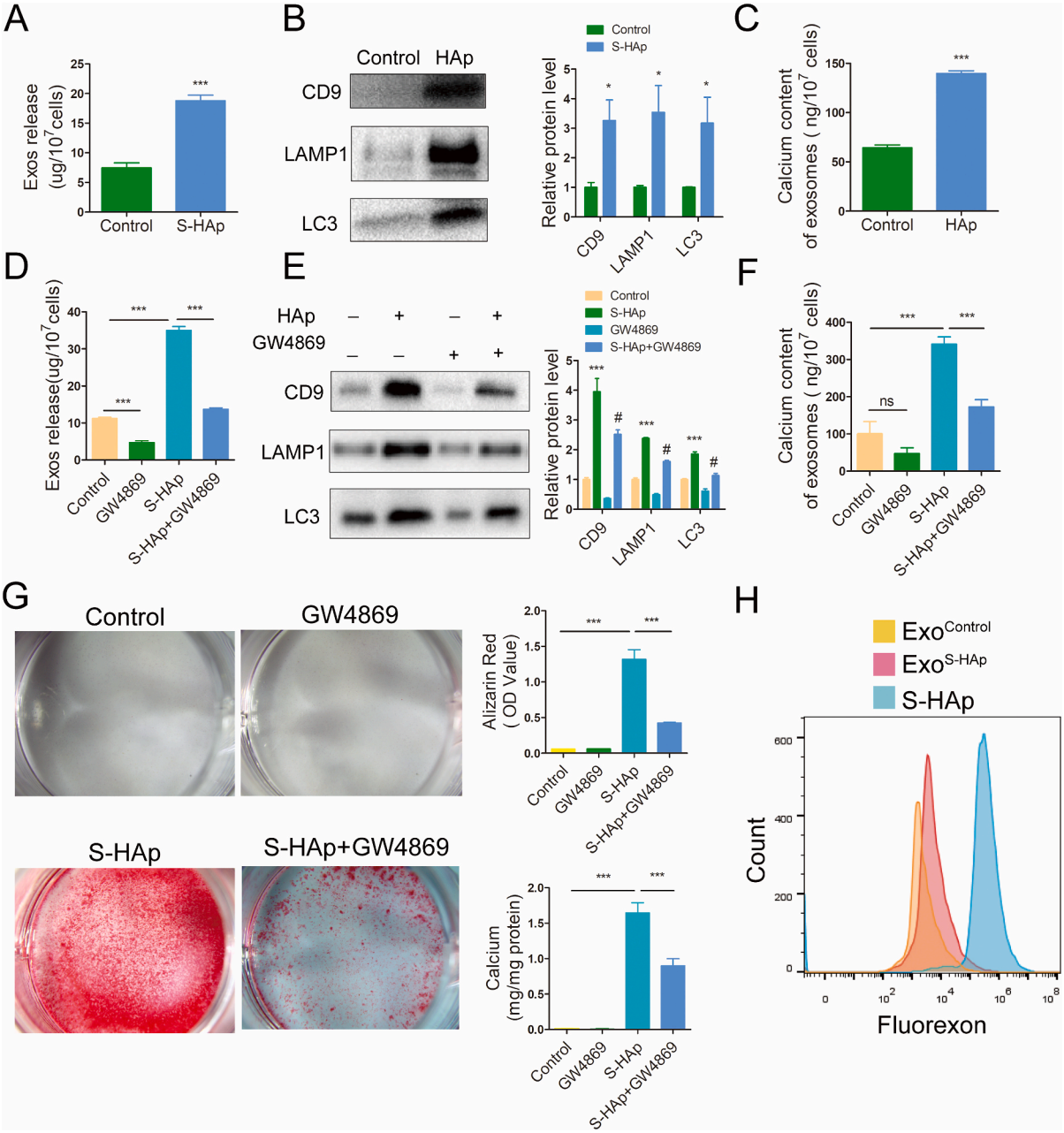

Fig. 9. Nano-HAp promoted release of exosomes which contained LC3 and LAMP1. A) Total protein was assessed in the Exos that were purified from the conditioned medium of VSMCs treated with or without S-HAp. B) Western Blot analysis for detection of CD9, LC3 and LAMP1 expression in the purified exosomes. Relative protein levels were quantified in comparison with the control. C) Calcium content in Exos was measured. D) Total protein was assessed in the Exos that were purified from the conditioned medium of VSMCs that were treated with 100 μg/mL S-HAp or/and 10 μm/L GW4869 for 3 days. E) Western blot analysis of CD9, LC3B and LAMP1. F) Analysis of calcium content of Exos that were treated with S-HAp or/and GW4869 for 5 days. Data are expressed as the mean ± SD. (*vs control, #vs HAp, $*p < 0.05$, $** p < 0.01$, $***p < 0.001$, $\#p < 0.05$). G) Alizarin red staining for calcification detection in VSMCs that were with S-HAp or/and GW4869 for 14 days. The bar graphs show the quantification of Alizarin red and the calcium content in the cells. Data are expressed as the mean ± SD. ($***p < 0.001$). H) FACS analysis of Exos from the conditioned medium of VSMCs treated with or without 100 μg/mL fluorexon-labeled S-HAp. The fluorexon labeled S-HAp was appointed as a positive control.

of internalized EGFR was impaired (Fig. 7A and B). Maturation of lysosomal protease CTSD was inhibited (Fig. 7E). Based on the dampened acidity of lysosome with a deficiency in CTSD maturation, we considered V-ATPase be a potential target of damage by nHAp. V-ATPases are membrane-embedded protein complexes that function as ATP hydrolysis-driven proton pumps. V-ATPases are the primary source of organellar acidification in all eukaryotes, making them essential for many fundamental cellular processes [47]. In our study, we detected a disruption in lysosomal anchoring of V-ATPase (Fig. 7F). Although further studies are required, our data first suggest that nHAp-caused defect of lysosomal acidification may involve impairment in V-ATPase transport to lysosomes. As nHAp blocks autophagy flux by impairing autolysosome degradation (Fig. 6), the accumulated autophagic vacuoles promoted calcium deposits. This was supported by our observation that either autophagy stimulator rapamycin or inhibitor CQ aggravated nHAp-induced calcification (Fig. 8A), and both had an additive effect on the accumulation of LC3 when they were used with nHAp (Fig 6B and Fig S7B). According to the above results, this may provide us new idea

that restoring lysosomal pH may control the progression of vascular calcification. cAMP is a multifunctional second messenger which controls extremely diverse and physiologically important biochemical pathways. Among its myriad roles, cAMP functions as an intracellular regulator of lysosomal pH, which is essential for the activity of acidic lysosomal enzymes [48]. Here we proved that cAMP attenuated the calcification caused by nHAp (Fig. 8E), indicating that blockage of autophagy flux indeed played a role in calcium deposits induced by nHAp.

Previous study proved that blocking autophagy promotes more rampant calcification by promoting release of MVs [49], and VSMC vesicle release contributed to calcification [50]. It has been shown that MVs played a central role in skeletal mineralization as they served as a nidus for initiation of hydroxyapatite crystal formation [51]. MVs were also identified in human aortic calcification, demonstrating that vascular calcification and bone mineralization occur by similar mechanisms [52]. Proteomic studies showed similarities between exosomes from VSMCs and skeletal osteoblasts, supporting that vascular calcification recapitulates skeletal mineralization [53]. We found that the exosomes released from VSMCs^{nHAp} contained more LC3 and LAMP1 than that from control VSMCs (Fig. 9B). It has been reported that more "calcifying" exosomes were secreted from VSMCs after pro-calcifying stimulation, which induced VC procession [49]. Calcium binds with Pi to form hydroxyapatite nodes on the inner and outside of "calcifying" exosomes membranes, which further initializes mineral deposition [49]. Nollet et al. found that autophagosomes from calcified mouse osteoblasts are packed with calcified hydroxyapatite [54]. Our study also showed there were HAp crystals in autophagosomes in VSMCs ^{nHAp} (Fig. 2F). Autophagic proteins were detected in MVs released from valve interstitial cells [20]. These results suggest that exosomes may have a crosstalk with the network of autophagic vesicles either at the stage of their formation or release during the process of VC [7]. Our study showed the accumulation of autophagosomes and autolysosomes, the enhancement of ALP activity and the increased release of exosomes from VSMCs induced by HAp. Based on these previous studies, we assume that the autophagic vesicles in VSMCs may be secreted out of the cells in the form of exosomes. We found that there were more exosomes released from VSMC^{HAp} as compared with the control (Fig 9A, Fig S14A&B), which resulted in more calcium contents released into ECM (Figs. 3B and 9C). GW4869 reduced not only the number of exosomes but also the protein content of LC3 and LAMP1, and calcium deposition as well (Fig. 9D–G). All these confirmed our postulation that accumulated autophagosomes and autolysosomes could be converted into calcium-containing exosomes that were released into ECM (Fig S15). This agrees with the report showing that VSMC calcification is mediated by regulated exosome secretion [24]. However, more studies are needed to further explore the relationship between autophagosomes and exosomes in regards the VC process. Our study unveiled that once nano-crystals were formed, they would facilitate the more rapid progression of calcification, showing the positive feedback of nHAp in the development of VC. Therapies aim to either prevent initial nHAp formation or nHAp-induced autophagy blockage or exosome releasing may be useful to control VC.

5. Conclusion

In summary, for the first time, we have shown that nHAp directly induces VC in vivo and blockage of autophagy flux participates in nHAp-accelerated calcification. We have identified that autophagy flux blockage results from lysosomal acidification inhibition, which then triggers release of calcifying exosomes from VSMCs and subsequent VC. Our results suggest that targeting this novel autophagy-lysosome-exosome pathway may help to control vascular calcification development.

Authors' contributions

QL and YL performed experiments, analyzed data, and prepared the manuscript; QL, YL, YZ and PPX analyzed data and prepared the figures; YZ, JYZ, PPX, WWJ, WJJ and MYC performed statistical analysis; RKT designed the experimental study, and revised the manuscript; HY designed the experimental study, prepared and revised the manuscript. All authors read and approved the final manuscript.

CRediT authorship contribution statement

Qi Liu: Conceptualization, Methodology, Validation, Formal analysis, Investigation, Writing – original draft, Writing – review & editing, Visualization. **Yi Luo:** Methodology, Validation, Investigation. **Yun Zhao:** Validation, Investigation. **Pingping Xiang:** Validation, Investigation. **Jinyun Zhu:** Writing – review & editing, Visualization. **Wangwei Jing:** Investigation. **Wenjing Jin:** Investigation. **Mingyao Chen:** Investigation. **Ruikang Tang:** Resources, Writing – review & editing, Supervision, Project administration. **Hong Yu:** Resources, Data curation, Writing – review & editing, Supervision, Project administration, Funding acquisition.

Declaration of competing interest

The authors declare no competing financial interest.

Acknowledgements

This work was supported by the National Natural Science Foundation of China Grant (No. 81570251 and NO.82070448 to HY).

Appendix A. Supplementary data

Supplementary data to this article can be found online at https://doi.org/10.1016/j.bioactmat.2021.06.004.

References

[1] R. Shroff, D.A. Long, C. Shanahan, Mechanistic insights into vascular calcification in CKD, J. Am. Soc. Nephrol. 24 (2) (2013) 179–189.
[2] R. Villa-Bellosta, A. Millan, V. Sorribas, Role of calcium-phosphate deposition in vascular smooth muscle cell calcification, Am. J. Physiol. Cell Physiol. 300 (1) (2011) C210–C220.
[3] L.L. Demer, Y. Tintut, Vascular calcification: pathobiology of a multifaceted disease, Circulation 117 (22) (2008) 2938–2948.
[4] Y. Liu, L. Zhang, Z. Ni, J. Qian, W. Fang, Calcium phosphate crystals from uremic serum promote osteogenic differentiation in human aortic smooth muscle cells, Calcif. Tissue Int. 99 (5) (2016) 543–555.
[5] L.W. Hunter, J.E. Charlesworth, S. Yu, J.C. Lieske, V.M. Miller, Calcifying nanoparticles promote mineralization in vascular smooth muscle cells: implications for atherosclerosis, Int. J. Nanomed. 9 (2014) 2689–2698.
[6] H. Liu, L.H. Huang, X.Y. Sun, J.M. Ouyang, High-phosphorus environment promotes calcification of A7R5 cells induced by hydroxyapatite nanoparticles, Mater Sci Eng C Mater Biol Appl 107 (2020) 110228.
[7] K. Phadwal, D. Feng, D. Zhu, V.E. MacRae, Autophagy as a novel therapeutic target in vascular calcification, Pharmacol. Ther. (2019) 107430.
[8] R. Chen, Y. Xu, W. Zhong, B. Li, P. Yang, Z.Q. Wang, C. Shao, C.P. Wang, J.C. Yan, Activation of CD137 signaling enhances vascular calcification through c-jun N-terminal kinase-dependent disruption of autophagic flux, Mediat. Inflamm. 2018 (2018) 8407137.
[9] D. Liu, W. Cui, B. Liu, H. Hu, J. Liu, R. Xie, X. Yang, G. Gu, J. Zhang, H. Zheng, Atorvastatin protects vascular smooth muscle cells from TGF-beta1-stimulated calcification by inducing autophagy via suppression of the beta-catenin pathway, Cell. Physiol. Biochem. 33 (1) (2014) 129–141.
[10] B. Frauscher, A.H. Kirsch, C. Schabhüttl, K. Schweighofer, M. Kétszeri, M. Pollheimer, D. Dragun, K. Schröder, A.R. Rosenkranz, K. Eller, P. Eller, Autophagy protects from uremic vascular media calcification, Front. Immunol. 9 (2018) 1866.
[11] A. Williams, S. Sarkar, P. Cuddon, E.K. Ttofi, S. Saiki, F.H. Siddiqi, L. Jahreiss, A. Fleming, D. Pask, P. Goldsmith, C.J. O'Kane, R.A. Floto, D.C. Rubinsztein, Novel targets for Huntington's disease in an mTOR-independent autophagy pathway, Nat. Chem. Biol. 4 (5) (2008) 295–305.

[12] I.G. Ganley, P.M. Wong, N. Gammoh, X. Jiang, Distinct autophagosomal-lysosomal fusion mechanism revealed by thapsigargin-induced autophagy arrest, Mol. Cell. 42 (6) (2011) 731–743.
[13] J.A. Mindell, Lysosomal acidification mechanisms, Annu. Rev. Physiol. 74 (2012) 69–86.
[14] S.T. Stern, P.P. Adiseshaiah, R.M. Crist, Autophagy and lysosomal dysfunction as emerging mechanisms of nanomaterial toxicity, Part. Fibre Toxicol. 9 (2012) 20.
[15] M.E. Papandreou, N. Tavernarakis, Autophagy and the endo/exosomal pathways in health and disease, Biotechnol. J. 12 (1) (2017).
[16] E.E. Golub, Role of matrix vesicles in biomineralization, Biochim. Biophys. Acta 1790 (12) (2009) 1592–1598.
[17] E.E. Golub, Biomineralization and matrix vesicles in biology and pathology, Semin. Immunopathol. 33 (5) (2011) 409–417.
[18] Z. Yin, C. Pascual, D.J. Klionsky, Autophagy: machinery and regulation, Microb Cell 3 (12) (2016) 588–596.
[19] T. Iwayama, T. Okada, T. Ueda, K. Tomita, S. Matsumoto, M. Takedachi, S. Wakisaka, T. Noda, T. Ogura, T. Okano, P. Fratzl, T. Ogura, S. Murakami, Osteoblastic lysosome plays a central role in mineralization, Sci Adv 5 (7) (2019), eaax0672.
[20] L. Cui, D.A. Houston, C. Farquharson, V.E. MacRae, Characterisation of matrix vesicles in skeletal and soft tissue mineralisation, Bone 87 (2016) 147–158.
[21] R. Buchet, S. Pikula, D. Magne, S. Mebarek, Isolation and characteristics of matrix vesicles, Methods Mol. Biol. 1053 (2013) 115–124.
[22] D.A. Chistiakov, V.A. Myasoedova, A.A. Melnichenko, A.V. Grechko, A.N. Orekhov, Calcifying matrix vesicles and atherosclerosis, BioMed Res. Int. 2017 (2017) 7463590.
[23] J.A. Leopold, Vascular calcification: mechanisms of vascular smooth muscle cell calcification, Trends Cardiovasc. Med. 25 (4) (2015) 267–274.
[24] A.N. Kapustin, M.L. Chatrou, I. Drozdov, Y. Zheng, S.M. Davidson, D. Soong, M. Furmanik, P. Sanchis, R.T. De Rosales, D. Alvarez-Hernandez, R. Shroff, X. Yin, K. Muller, J.N. Skepper, M. Mayr, C.P. Reutelingsperger, A. Chester, S. Bertazzo, L. J. Schurgers, C.M. Shanahan, Vascular smooth muscle cell calcification is mediated by regulated exosome secretion, Circ. Res. 116 (8) (2015) 1312–1323.
[25] A.E. Ewence, M. Bootman, H.L. Roderick, J.N. Skepper, G. McCarthy, M. Epple, M. Neumann, C.M. Shanahan, D. Proudfoot, Calcium phosphate crystals induce cell death in human vascular smooth muscle cells: a potential mechanism in atherosclerotic plaque destabilization, Circ. Res. 103 (5) (2008) e28–34.
[26] C. Théry, S. Amigorena, G. Raposo, A. Clayton, Isolation and characterization of exosomes from cell culture supernatants and biological fluids, Curr Protoc Cell Biol Chapter 3 (2006). Unit 3.22.
[27] S.W. Ha, H.L. Jang, K.T. Nam, G.R. Beck Jr., Nano-hydroxyapatite modulates osteoblast lineage commitment by stimulation of DNA methylation and regulation of gene expression, Biomaterials 65 (2015) 32–42.
[28] L. Yu, Y. Chen, S.A. Tooze, Autophagy pathway: cellular and molecular mechanisms, Autophagy 14 (2) (2018) 207–215.
[29] J. Pang, H. Peng, S. Wang, X. Xu, F. Xu, Q. Wang, Y. Chen, L.A. Barton, Y. Chen, Y. Zhang, J. Ren, Mitochondrial ALDH2 protects against lipopolysaccharide-induced myocardial contractile dysfunction by suppression of ER stress and autophagy, Biochim. Biophys. Acta (BBA) - Mol. Basis Dis. 1865 (6) (2019) 1627–1641.
[30] S. Bertazzo, E. Gentleman, K.L. Cloyd, A.H. Chester, M.H. Yacoub, M.M. Stevens, Nano-analytical electron microscopy reveals fundamental insights into human cardiovascular tissue calcification, Nat. Mater. 12 (6) (2013) 576–583.
[31] G. Campi, F. Cristofaro, G. Pani, M. Fratini, B. Pascucci, P.A. Corsetto, B. Weinhausen, A. Cedola, A.M. Rizzo, L. Visai, G. Rea, Heterogeneous and self-organizing mineralization of bone matrix promoted by hydroxyapatite nanoparticles, Nanoscale 9 (44) (2017) 17274–17283.
[32] C. Liu, H. Zhai, Z. Zhang, Y. Li, X. Xu, R. Tang, Cells recognize and prefer bone-like hydroxyapatite: biochemical understanding of ultrathin mineral platelets in bone, ACS Appl. Mater. Interfaces 8 (44) (2016) 29997–30004.
[33] S.-W. Ha, J. Park, M.M. Habib, G.R. Beck, Nano-hydroxyapatite stimulation of gene expression requires fgf receptor, phosphate transporter, and erk1/2 signaling, ACS Appl. Mater. Interfaces 9 (45) (2017) 39185–39196.
[34] F. Bezerra, M.R. Ferreira, G.N. Fontes, C.J. da Costa Fernandes, D.C. Andia, N. C. Cruz, R.A. da Silva, W.F. Zambuzzi, Nano hydroxyapatite-blasted titanium surface affects pre-osteoblast morphology by modulating critical intracellular pathways, Biotechnol. Bioeng. 114 (8) (2017) 1888–1898.
[35] S. Cao, H. Li, K. Li, J. Lu, L. Zhang, In vitro mineralization of MC3T3-E1 osteoblast-like cells on collagen/nano-hydroxyapatite scaffolds coated carbon/carbon composites, J. Biomed. Mater. Res. 104 (2) (2016) 533–543.
[36] K. Zhou, P. Yu, X. Shi, T. Ling, W. Zeng, A. Chen, W. Yang, Z. Zhou, Hierarchically porous hydroxyapatite hybrid scaffold incorporated with reduced graphene oxide for rapid bone ingrowth and repair, ACS Nano 13 (8) (2019) 9595–9606.
[37] A.P. Sage, J. Lu, Y. Tintut, L.L. Demer, Hyperphosphatemia-induced nanocrystals upregulate the expression of bone morphogenetic protein-2 and osteopontin genes in mouse smooth muscle cells in vitro, Kidney Int. 79 (4) (2011) 414–422.
[38] V.M. Miller, G. Rodgers, J.A. Charlesworth, B. Kirkland, S.R. Severson, T. E. Rasmussen, M. Yagubyan, J.C. Rodgers, F.R. Cockerill 3rd, R.L. Folk, E. Rzewuska-Lech, V. Kumar, G. Farell-Baril, J.C. Lieske, Evidence of nanobacterial-like structures in calcified human arteries and cardiac valves, Am. J. Physiol. Heart Circ. Physiol. 287 (3) (2004) H1115–H1124.
[39] D. Yamanouchi, S. Morgan, C. Stair, S. Seedial, J. Lengfeld, K.C. Kent, B. Liu, Accelerated aneurysmal dilation associated with apoptosis and inflammation in a newly developed calcium phosphate rodent abdominal aortic aneurysm model, J. Vasc. Surg. 56 (2) (2012) 455–461.
[40] Y.Q. Peng, D. Xiong, X. Lin, R.R. Cui, F. Xu, J.Y. Zhong, T. Zhu, F. Wu, M.Z. Mao, X. B. Liao, L.Q. Yuan, Oestrogen inhibits arterial calcification by promoting autophagy, Sci. Rep. 7 (1) (2017) 3549.
[41] W.E. Hughes, A.M. Beyer, Vascular autophagy in physiology and pathology, Am. J. Physiol. Heart Circ. Physiol. 316 (1) (2019) H183–h185.
[42] R. Wang, H. Hu, J. Guo, Q. Wang, J. Cao, H. Wang, G. Li, J. Mao, X. Zou, D. Chen, W. Tian, Nano-hydroxyapatite modulates osteoblast differentiation through autophagy induction via mTOR signaling pathway, J. Biomed. Nanotechnol. 15 (2) (2019) 405–415.
[43] J. Wang, Y. Yu, K. Lu, M. Yang, Y. Li, X. Zhou, Z. Sun, Silica nanoparticles induce autophagy dysfunction via lysosomal impairment and inhibition of autophagosome degradation in hepatocytes, Int. J. Nanomed. 12 (2017) 809–825.
[44] X. Zhao, S. Wei, Z. Li, C. Lin, Z. Zhu, D. Sun, R. Bai, J. Qian, X. Gao, G. Chen, Z. Xu, Autophagic flux blockage in alveolar epithelial cells is essential in silica nanoparticle-induced pulmonary fibrosis, Cell Death Dis. 10 (2) (2019) 127.
[45] Y. Cai, X.L. Wang, A.M. Flores, T. Lin, R.J. Guzman, Inhibition of endo-lysosomal function exacerbates vascular calcification, Sci. Rep. 8 (1) (2018) 3377.
[46] R. Sudo, F. Sato, T. Azechi, H. Wachi, 7-Ketocholesterol-induced lysosomal dysfunction exacerbates vascular smooth muscle cell calcification via oxidative stress, Gene Cell. 20 (12) (2015) 982–991.
[47] T. Vasanthakumar, J.L. Rubinstein, Structure and roles of V-type ATPases, Trends Biochem. Sci. 45 (4) (2020) 295–307.
[48] C. Maity, D. Ghosh, S. Guha, Assays for intracellular cyclic adenosine monophosphate (cAMP) and lysosomal acidification, Methods Mol. Biol. (2019) 161–178, 1996.
[49] C. Zhang, K. Zhang, F. Huang, W. Feng, J. Chen, H. Zhang, J. Wang, P. Luo, H. Huang, Exosomes, the message transporters in vascular calcification, J. Cell Mol. Med. 22 (9) (2018) 4024–4033.
[50] J.L. Reynolds, A.J. Joannides, J.N. Skepper, R. McNair, L.J. Schurgers, D. Proudfoot, W. Jahnen-Dechent, P.L. Weissberg, C.M. Shanahan, Human vascular smooth muscle cells undergo vesicle-mediated calcification in response to changes in extracellular calcium and phosphate concentrations: a potential mechanism for accelerated vascular calcification in ESRD, J. Am. Soc. Nephrol. 15 (11) (2004) 2857–2867.
[51] H.C. Anderson, Vesicles associated with calcification in the matrix of epiphyseal cartilage, J. Cell Biol. 41 (1) (1969) 59–72.
[52] H.C. Anderson, Mineralization by matrix vesicles, Scanning Electron. Microsc. (Pt 2) (1984) 953–964.
[53] Y. Tintut, L.L. Demer, Exosomes: nanosized cellular messages, Circ. Res. 116 (8) (2015) 1281–1283.
[54] M. Nollet, S. Santucci-Darmanin, V. Breuil, R. Al-Sahlanee, C. Cros, M. Topi, D. Momier, M. Samson, S. Pagnotta, L. Cailleteau, S. Battaglia, D. Farlay, R. Dacquin, N. Barois, P. Jurdic, G. Boivin, D. Heymann, F. Lafont, S.S. Lu, D. W. Dempster, G.F. Carle, V. Pierrefite-Carle, Autophagy in osteoblasts is involved in mineralization and bone homeostasis, Autophagy 10 (11) (2014) 1965–1977.